Water Quality and Mass Transport in Four Watersheds in Eastern Puerto Rico

By Robert F. Stallard and Sheila F. Murphy

Chapter E of
Water Quality and Landscape Processes of Four Watersheds in Eastern Puerto Rico
Edited by Sheila F. Murphy and Robert F. Stallard

Professional Paper 1789–E

U.S. Department of the Interior
U.S. Geological Survey

Contents

Figures

Tables

Abbreviations Used in This Report

>	greater than
—	preceding a compound, such as $-PO_4^{3-}$, indicates likelihood of linkage to a cation
µm	micrometer
µS cm^{-1}	microsiemens per centimeter
km	kilometer
km^2	square kilometer
mm	millimeter
mm h^{-1}	millimeters per hour
mm yr^{-1}	millimeters per year
t km^{-2} yr^{-1}	metric tons per square kilometer per year
DOC	dissolved organic carbon
SI	saturation index
WEBB	Water, Energy, and Biogeochemical Budgets

Conversion Factors

Multiply	By	To obtain
	Length	
micrometer (μm)	0.00003937	inch (in.)
millimeter (mm)	0.03937	inch (in.)
kilometer (km)	0.6214	mile (mi)
	Area	
square kilometer (km^2)	0.3861	square mile (mi^2)
	Flow rate	
millimeters per hour (mm h^{-1})	0.03937	inches per year (in. h^{-1})
millimeters per year (mm yr^{-1})	0.03937	inches per year (in. yr^{-1})
	Specific Conductance	
microsiemens per centimeter (μS cm^{-1})	1.000	micromho per centimeter (μmho cm^{-1})
	Other	
metric tons per square kilometer per year (t km^{-2} yr^{-1})	2.855	short tons per square mile per year (tons mi^{-2} yr^{-1})

Water Quality and Mass Transport in Four Watersheds in Eastern Puerto Rico

By Robert F. Stallard and Sheila F. Murphy

Abstract

Water quality of four small watersheds in eastern Puerto Rico has been monitored since 1991 as part of the U.S. Geological Survey's Water, Energy, and Biogeochemical Budgets program. These watersheds represent a montane, humid-tropical environment and differ in geology and land cover. Two watersheds are located on granitic rocks, and two are located on volcaniclastic rock. For each bedrock type, one watershed is covered with mature rainforest in the Luquillo Mountains, and the other watershed is undergoing reforestation after being affected by agricultural practices typical of eastern Puerto Rico. A subwatershed of the Icacos watershed, the Guabá, was also monitored to examine scaling effects. The water quality of the rivers draining forest, in the Icacos and Guabá (granitic watersheds) and Mameyes (a volcaniclastic watershed), show little contamination by human activities. The water is well oxygenated and has a nearly neutral pH, and nutrient concentrations are low. Concentrations of nutrients in the disturbed watersheds, the Cayaguás (granitic rock) and Canóvanas (volcaniclastic rock), are greater than in the forested watersheds, indicating some inputs from human activities. High in-stream productivity in the Canóvanas watershed leads to occasional oxygen and calcite supersaturation and carbon dioxide undersaturation. Suspended sediment concentrations in all watersheds are low, except during major storms. Most dissolved constituents derived from bedrock weathering or atmospheric deposition (including sodium, magnesium, calcium, silica, alkalinity, and chloride) decrease in concentration with increasing runoff, reflecting dilution from increased proportions of overland or near-surface flow. Strongly bioactive constituents (dissolved organic carbon, potassium, nitrate, ammonium ion, and phosphate) commonly display increasing concentration with increasing runoff, regardless of their ultimate origin (bedrock or atmosphere). The concentrations of many of the bioactive constituents eventually decrease at runoff rates greater than 3 to 10 millimeters per hour, presumably reflecting an increased relative contribution from overland flow. Sulfate behaves like the nonbioactive constituents in the Canóvanas, Cayaguás, and Mameyes watersheds but like a bioactive constituent in the Icacos and Guabá watersheds. Storms resulted in several anomalous sample compositions. Runoff waters from a number of storms—mostly hurricanes, but also other storms—have exceptionally high chloride concentrations, presumably resulting from windborne seasalt from the ocean, and low nitrate concentrations, reflecting a dominance of maritime air masses contributing moisture to the storms. High-potassium samples, without high chloride, are also associated with some smaller storms that followed Hurricane Georges in 1998; they are likely related to the breakdown of fallen vegetation. Finally, occasional low-silica events are observed in the Icacos and Guabá watersheds in the years prior to Hurricane Georges, but not after; this difference may be related to a change in hydrologic flow paths.

Introduction

The U.S. Geological Survey initiated the Water, Energy, and Biogeochemical Budgets (WEBB) program in 1990 to study water, energy, and biogeochemical fluxes and interactions throughout a range of temporal and spatial scales (Lins, 1994). The WEBB site in eastern Puerto Rico represents a montane, humid-tropical environment with a bedrock geology typical of many parts of the world, and it therefore provides an excellent platform for obtaining a better understanding of processes that control the composition of water in other tropical environments (Larsen and others, 1993). At the Puerto Rico site, four watersheds with different geology and land cover can be compared (Murphy and others, 2012). Two watersheds are located on coarse-grained granitic rocks (Icacos and Cayaguás), and two are located on fine-grained volcanic and volcaniclastic rocks (Mameyes and Canóvanas). For each bedrock type, one watershed is covered with mature forest (Icacos and Mameyes), and the other watershed has been affected by agricultural land use typical of eastern Puerto Rico (Cayaguás and Canóvanas). In addition, a subwatershed of the Icacos watershed, the Guabá, was studied to examine scaling effects.

The warm, wet Luquillo Mountains of eastern Puerto Rico are the headwaters of numerous streams and rivers, including the Río Icacos and Río Mameyes (fig. 1). Visitors to the El Yunque National Forest (which is contiguous with the Luquillo Experimental Forest) typically visit the forest during calm weather, when rivers are clear and gently flowing over their beds. This water has a neutral pH and is well oxygenated,

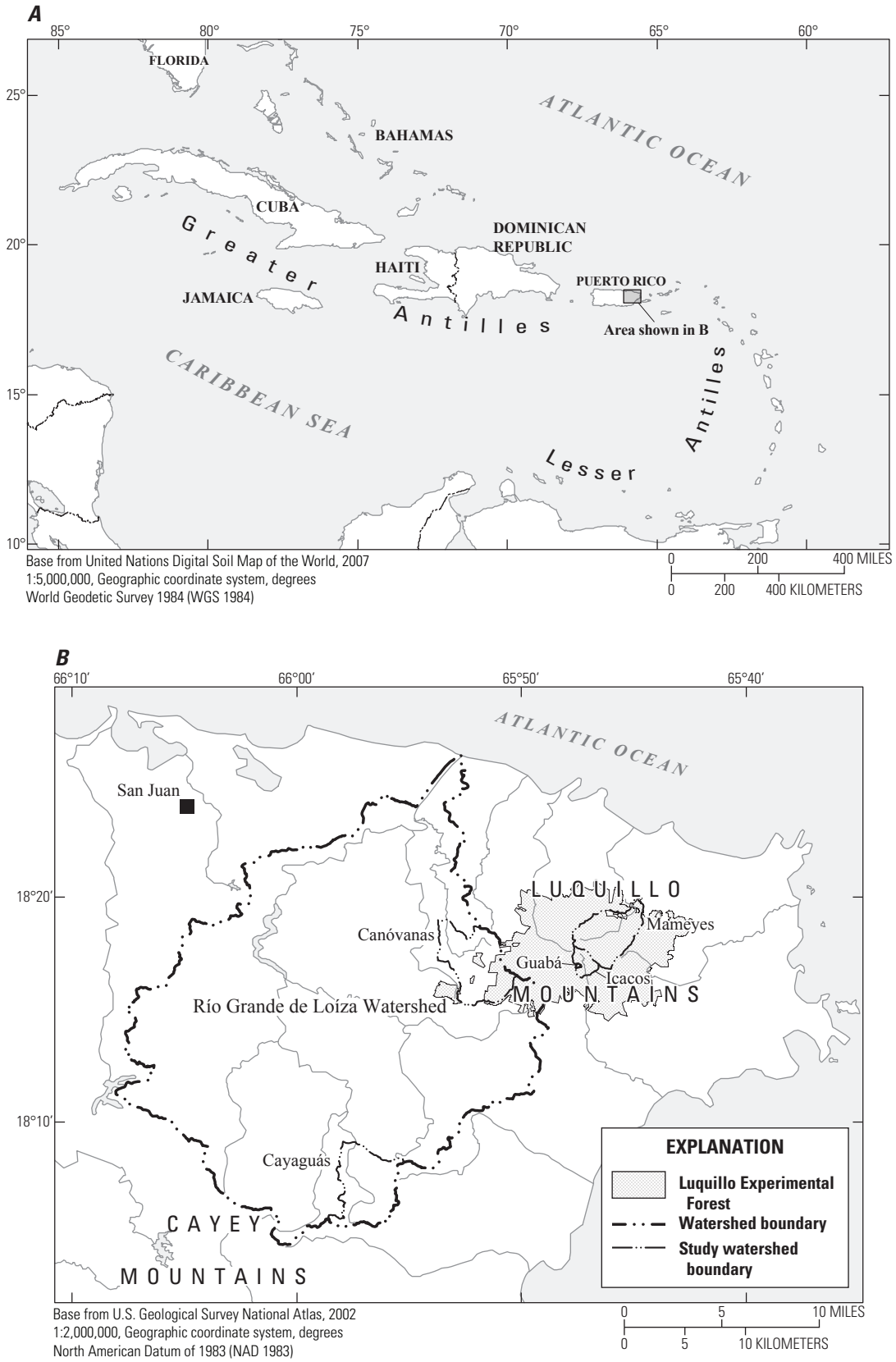

Figure 1. Location of Puerto Rico and study watersheds, eastern Puerto Rico.

and if it is treated to make it potable, it is quite delicious—presumably being flavored by the chemical breakdown of bedrock, a little seasalt, and bit of dissolved organic matter. Most visitors avoid the forest during intense storms, such as hurricanes and major cold fronts, which turn the rivers into muddy, raging torrents that threaten life and infrastructure. Sometimes so much rain falls that entire hillslopes of soil crash down in landslides. Occasionally, winds are so strong that forest vegetation is shredded and large quantities of salt spray from the ocean are blown over the forest. Less visible contributions to the forest are made by atmospheric deposition; nitrogen in rainfall has almost doubled since it was first monitored in 1985 (Stallard, 2012a). A fungus has led to a die-off of some endemic frogs, and droughts and pollution from North America, Europe, and Africa may have increased the virulence of the infection (Stallard, 2001; Burrowes and others, 2004).

The Río Grande de Loíza watershed drains the western flank of the Luquillo Mountains and the flatter area to the west (fig. 1). Deforestation for hundreds of years (Gould and others, 2012; Murphy and others, 2012) and the construction of roads in steep terrain have increased surface runoff and sediment delivery to streams (Larsen and Parks, 1997; Clark and Wilcock, 2000). As Puerto Rico has urbanized during the past half century, much of the island's previously denuded lands, including the Cayaguás and Canóvanas watersheds, are undergoing reforestation; however, stored sediment continues to be released to the reservoirs and the ocean during floods (Webb and Soler-López, 1997; Larsen and Santiago-Román, 2001). The water quality of rivers in the recovering landscape is affected by runoff from remaining agricultural lands and waste from domestic and industrial sources.

Factors Affecting Water Chemistry of Tropical Rivers

The processes by which river waters acquire their composition, as related to the movement of water through soil and its interaction with the overlying vegetation and underlying bedrock, are an area of active research. Previous studies of large tropical rivers (Gibbs, 1967, 1972; Stallard and Edmond, 1981, 1983, 1987; Stallard, 1985, 1988; Lewis and others, 1987; Saunders and Lewis, 1988, 1989; 1990; Fox, 1989, 1993; Lewis and Saunders, 1989; Stallard and others, 1991; Devol and others, 1995; Edmond and others, 1995, 1996; Tardy and others, 2005, 2009) and of the Luquillo Mountains (McDowell and others, 1990, 1996; McDowell, 1991, 1998; Lodge and others, 1994; McDowell and Asbury, 1994; Chestnut and others, 1999; Aitkenhead and McDowell, 2000; Chestnut and McDowell, 2000; Zeigler and others, 2005; Derry and others, 2006; Peters and others, 2006; Bhatt and McDowell, 2007; Heartsill-Scalley and others, 2007; Pett-Ridge, 2009; Pett-Ridge and others, 2009a,b; Shanley and others, 2011) demonstrate that it is possible to classify and organize river-borne chemical constituents on the basis of their primary sources and bioactivity. Constituents that are largely bedrock derived include calcium (Ca^{2+}), alkalinity, silica ($Si(OH)_4$), and phosphate ($-PO_4^{3-}$). Phosphate is susceptible to attaching to aluminum and iron oxides and hydroxides and being lost from solution, and the preceding "–" indicates linkages with other constituents such as iron, aluminum, and organic matter. Chloride (Cl^-) and sulfate (SO_4^{2-}) are largely of seasalt origin; additional SO_4^{2-} comes from the weathering of sulfide minerals, sometimes exposed through mining, and from atmospheric sulfuric acid, which has both natural and combustion sources. The cations sodium (Na^+), potassium (K^+), and magnesium (Mg^{2+}) are predominantly bedrock derived, with lesser seasalt contributions. Siliceous bedrock is a source of all of the bedrock-derived constituents, and Na^+-bearing and Ca^{2+}-bearing bedrock-forming minerals weather the most rapidly and completely. Where present, carbonate minerals are strong sources of Ca^{2+}, alkalinity, and sometimes Mg^{2+}. Several constituents, such as nitrate (NO_3^-), ammonium ion (NH_4^+), and dissolved organic carbon (DOC), are ultimately derived from atmospheric gases that have chemical, biological, and sometimes anthropogenic origins.

Biological processes associated with the growth and maintenance of a forest can have a considerable effect on the ultimate chemical composition of that water. The classic model of nutrient cycling in tropical rainforests (Herrera and others, 1978a,b; Stark and Jordan, 1978; invoked for Luquillo by McDowell, 1998, 2001) is a tight, vertical, almost-closed cycle where nutrients released from vegetation by throughfall or decay are efficiently recovered by plant roots and reincorporated into vegetation as water moves through the upper soil profile. Of the constituents studied here, K^+, SO_4^{2-}, DOC, NO_3^-, NH_4^+, and $-PO_4^{3-}$, are strongly bioactive, and biological processes, including this internal cycling, can have a profound effect on their distribution in surface waters. The bioactivity of these constituents is manifested by a strong enrichment in throughfall (water that has interacted with leaves and branches) compared with rainfall (Heartsill-Scalley and others, 2007) and in streams following hurricanes (McDowell and others, 1996; Schaefer and others, 2000; Shanley and others, 2011). Sulfate, DOC, NO_3^-, and NH_4^+ can be also be lost to the atmosphere through transformation back into various gases. All of the biologically active constituents have domestic and agricultural sources.

The chemistry of underlying bedrock is a controlling factor of the water chemistry of any river. In Puerto Rico's WEBB program watersheds, the two rock types primarily differ in their quartz content: the granitic rocks typically contain between 20 and 33 percent quartz, whereas the volcaniclastic rocks have little or no quartz (Murphy and others, 2012). The presence of quartz in bedrock leads to a sandy texture in overlying soils and tends to increase their ability to transmit water (Murphy and Stallard, 2012). Where quartz is absent, as in volcanic bedrock, sand-sized grains in associated soils and river sediments are rare (Johnsson and Stallard, 1989; Johnsson, 1990), and soils are typically finer grained and have lower permeability and infiltration rates (Simon and others, 1990).

The presence or absence of quartz in bedrock is clearly evident in the channel forms of eastern Puerto Rico rivers (see cover photograph). The two WEBB study-area rivers that drain quartz-poor, volcaniclastic rocks (Mameyes and Canóvanas) have abundant exposed bedrock, bouldery beds, and poorly developed flood plains and riparian areas. Many nooks and crannies shelter aquatic creatures. In contrast, the rivers that drain granitic rocks (Icacos, Cayaguás, and Guabá) have beds of quartz sand, well-developed flood plains, and extensive riparian areas, especially where their stream gradients are gentler. Their channels support hyporheic flow, and the flood plains and riparian areas can modify water quality.

When quartz chemically weathers, it produces only dissolved silica ($Si(OH)_4$), which is a common weathering product of many silicate minerals. Therefore, quartz dissolution is difficult to differentiate from other reactions when one examines solute composition alone (pitted quartz surfaces, which have been observed on grains from the Icacos watershed, have been used to identify dissolution; Brantley and others, 1986; Schulz and White, 1999). If quartz is ignored, the remaining minerals in the granitic and volcaniclastic bedrock types are similar, with a slight bias to more Mg- and Ca-rich minerals in the volcaniclastic rocks (Smith and others, 1998, their fig. 3, table 2). Therefore, solute signatures from weathering of the granitic or volcaniclastic rocks should be similar. Differences in solute composition, however, can be caused by other rock types, such as carbonate rocks, sulfide ores, and ultramafic rocks, or by indirect effects, such as different rates and pathways for water movement through soils and the presence or absence of riparian areas.

The interaction between water, soil, and bedrock, as manifested by the relation between concentration (C) and runoff rate (R), appears to be similar in a wide range of rivers, indicating a commonality in the physical and chemical mechanisms that mobilize and export solutes from watersheds. Godsey and others (2009) compare data from the U.S. Geological Survey Hydrologic Benchmark Network for 59 small, geochemically diverse watersheds in the United States in landscapes that are not heavily affected by human activities. They focused on chemical constituents that are derived from bedrock weathering and are not biologically active—Na^+, Ca^{2+}, Mg^{2+}, and $Si(OH)_4$—and looked for crosscutting patterns that would provide insight as to how these constituents were acquired by the streams.

Godsey and others (2009) note that most streams demonstrated a linear relation between $\log(C)$ and $\log(R)$,

$$\log(C) = a + b \bullet \log(R),$$

where a is a constant and b is a slope. A zero slope implies a fixed concentration and is termed a "chemostat," whereas a slope of −1 implies a constant input rate of the constituent, independent of runoff. A positive slope implies that increasing rainfall and runoff serve to mobilize the constituent. For Na^+, Ca^{2+}, Mg^{2+}, and $Si(OH)_4$, b is typically negative, mostly between −0.05 and −0.15 and is statistically different from zero. The slightly negative slope is close to being a chemostat, implying that subsoil processes substantially increase the supply of these constituents in response to more water flowing through the soil and that many watersheds respond in a similar way, despite marked differences in geology, vegetation, and climate.

Godsey and others (2009) compared three simple models that each successfully reproduce nearly log-linear relations between runoff and constituent concentration. For two of these models, the Hubbard Brook "working model" of Johnson and others (1969) and the rapid, flow-through-reaction model of Langbein and Dawdy (1964), the model relation has a sigmoidal shape, leveling off at low and high runoff rates. Successful models require that the concentrations of constituents in the input to the soil reservoir greatly exceed those of rainwater and could be thought of as soil-water concentrations. The authors also develop their own strictly log-linear model, the "permeability-porosity-aperture" model. This model assumes that permeability, porosity, and average pore aperture decrease exponentially with depth; precipitation rates are approximately the same across a hillslope; flows through the watershed behave according to Darcy's Law; minimal flows originate near the divide and the stream; and solute flux is proportional to reactive surface area such that secondary and back-reactions do not control solute fluxes (Godsey and others, 2009). The model handles stored water.

The slope, b, of the permeability-porosity-aperture model is derived from the depth-dependent e-folding lengths of four different structural and chemical properties. The model predicts that b should be the same for all bedrock-derived constituents, although the authors allow that differences for slopes among various constituents could be attributable to differences in the depth distribution of reactive minerals throughout the soil profile. The authors also caution against trying to derive b from field measurements, stating "Any such attempt at direct measurement [of the properties that go into determining the slope] would be complicated by the spatial heterogeneity in subsurface properties, as well as the large differences between field and laboratory weathering rates."

During big storms, water does not necessarily flow through the soil profile. Storm events play a major, often dominant, role in the mobilization of river-borne materials from hillslopes and stream channels and in the transport of these materials downriver (Wolman and Miller, 1960). In tropical, high-runoff settings, near-surface and overland flow can be more important than soil infiltration during storms (Elsenbeer, 2001, Godsey and others, 2004). Elsenbeer (2001) developed a simplified classification scheme based on infiltration styles (fig. 2). When rainfall intensities for a given locale exceed the hydrologic conductivity (K_{sat}) in the shallow parts of the soil profile, water is shunted into shallower, lateral flow paths or into overland flow. In hilly watersheds with shallow bedrock or impermeable soils (Acrisols), surface lateral flow of water will predominate (fig. 2), because K_{sat} decreases rapidly in the soil profile (a change of 2 or 3 orders of magnitude in the first meter of soil). In contrast, in watersheds with deep, porous

soils (Ferralsols), K_{sat} remains high through the soil profile (a change of 1 order of magnitude or less in the first meter of soil), and deep infiltration is likely. In Acrisols, water and nutrients can both leave the watershed during storms before ever interacting with soil and roots.

For all soils, pipes and macropores (large-diameter connected flow paths characteristically produced by soil cracks, decayed roots, and burrows) can be sufficiently abundant that they dominate infiltration and lateral shallow-soil flow. Shallow-soil, overland, macropore, and pipe flow all provide pathways for water and solutes that modify interaction with plant roots, especially during large storms (Beven and Germann, 1982; Elsenbeer and Cassel, 1990; Elsenbeer and Lack, 1996; Elsenbeer and others, 1996; Godsey and others, 2004, Kinner and Stallard, 2004; Chappell and others, 2005; Larsen and others, 2012). In fact, macropore effects can dominate soil-matrix flow at hillslope scale, considerably changing how a soil might be classified according to figure 2 (Chappell and others 1998, 2005).

The most intense rainfall events in eastern Puerto Rico occur during hurricanes and large frontal storms. These large storms shred and topple vegetation, generate landslides that strip soils and vegetation off slopes, and substantially alter stream-water chemistry (McDowell and others, 1996; Schaefer and others, 2000; Heartsill-Scalley and others, 2007; Larsen, 2012). Although granitic soils have greater groundwater storage and somewhat faster infiltration (Murphy and Stallard, 2012), in both the Mameyes and Icacos watersheds, high runoff rates produce substantial overland flow on forested soils on both granitic and volcaniclastic bedrock as well as on fresh and recovering landslides (Larsen, 2012), indicating Acrisol-type soil hydrology in both types of bedrock.

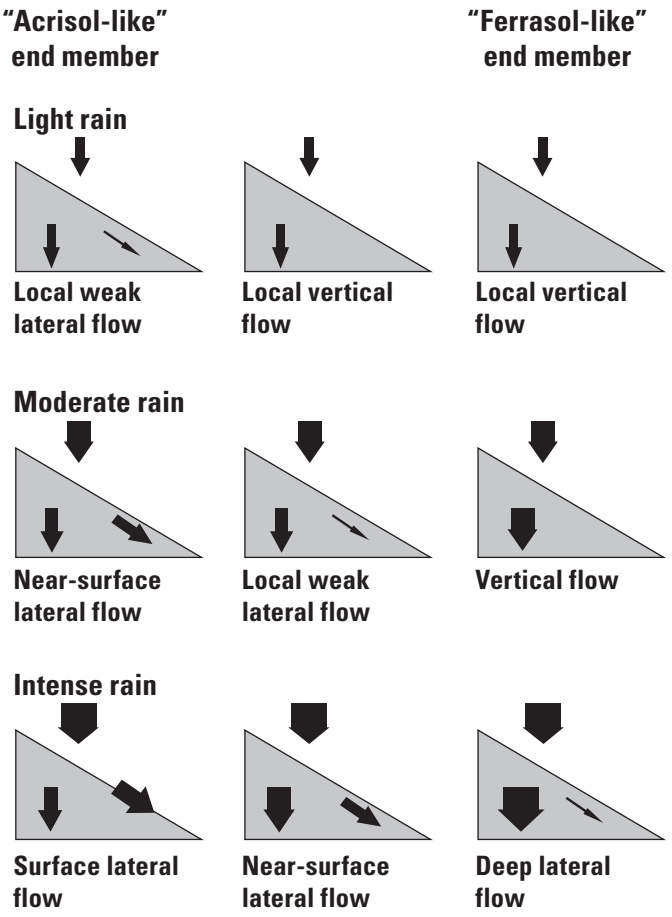

Figure 2. Adaptation of Elsenbeer's (2001) functional classification of tropical forest watersheds according to prevailing hydrological flow paths, based on measured saturated hydraulic conductivities (K_{sat}). Each row represents soil response under different rainfall intensities. Arrows indicate movement of water overland and through soil; thickness of arrows indicates approximate relative proportions. For light rain, much moisture does not get to the stream and is probably lost through transpiration. Surface lateral flow is encountered in hilly watersheds with shallow bedrock or impermeable soils (left diagram), where K_{sat} typically decrease rapidly in the profile and rainfall is intense. Deep lateral flow (right diagram) occurs where K_{sat} do not decrease rapidly in the profile. Note that Acrisols are roughly equivalent to Ultisols in the United States soil classification and Ferralsols are roughly equivalent to Oxisols (Soil Survey Staff, 1995), and that macropores normally complicate the role of matrix porosity (Chappell and others, 1998; Chappell and Sherlock, 2005).

Study Design and Objectives

This chapter presents water chemistry for thousands of samples collected during the first 15 years (1991–2005) of the Puerto Rico WEBB program. The data, which are available from the U.S. Geological Survey's National Water Information System website (*http://nwis.waterdata.usgs.gov/usa/nwis/qwdata*), provide a unique opportunity to examine the composition of stream water during storms. We are not aware of any published data anywhere in the world for water samples collected at runoff rates greater than 20 millimeters per hour (mm h^{-1}) that have been analyzed for chemistry and suspended sediment (appendix 1). The Hydrologic Benchmark Network dataset examined by Godsey and others (2009) contains comprehensive chemistry for only 30 samples, from 12 rivers, that were sampled at runoff rates greater than 1 mm h^{-1}; of these, the maximum runoff rate was 5.9 mm h^{-1}. The eastern Puerto Rico WEBB study analyzed comprehensive chemistry in 543 samples collected at runoff rates greater than 1 mm h^{-1}, 256 samples at greater than 10 mm h^{-1}, and 3 samples at greater than 90 mm h^{-1}. Because the soils of the study watersheds generally behave like Acrisols (Murphy and Stallard, 2012), strong, downslope, near-surface water flow and concomitant

nutrient export are expected during storms. The models presented by Godsey and others (2009) are for water moving through soil; thus, at the high-flow regimes sampled during the WEBB study, deviations from linear trends of log(C) compared with log(R) might be expected because different flow paths are active.

In this report, we use the relation between constituent concentration and discharge as a basis for examining processes operating at different flow regimes. Similar to the approach used by Godsey and others (2009), we examined the structure of the primary data graphically and through fitting simple regressions to the data, and we compared these results among study rivers and with the results of other studies. We also estimated continuous rates of watershed export (loads) of each constituent and averaged the loads for ranges of discharge in order to construct averaged constituent-discharge relations. We asked: (1) Do we see nonlinear features in the high-runoff samples in this dataset that are not seen elsewhere, such as in the Hydrologic Benchmark Network's summary of Godsey and others (2009)? (2) How do atmospherically derived and biologically active constituents differ from largely bedrock-derived constituents? And, (3) Do we see features in these data comparisons that can be used to inform the selection of models for describing the biogeochemistry of tropical and other watersheds? To ask these questions, we performed a set of tests:

- Does each constituent show similar behavior among all sites?
- Do all bedrock-derived constituents have nearly linear relations between log(C) and log(R)?
- For a given river or for rivers with similar watershed geology, are the slopes similar for all bedrock-derived constituents?
- If slopes are not similar, are they arrayed according to the reactivity of the parent minerals in the soil profile, or in some other biogeochemically consistent manner?
- Do differences of slopes in the linear relations between log(C) and log(R) among rivers relate to geology, supporting an assumption that soil porosity and pore openings, and their vertical distribution, are controlled by geology?
- Is there a breakdown in the log-linear relation (curvature) at high flow, indicating that other flow paths are active?
- Do bioactive constituents show concentration-runoff relations that reflect their increased abundance in the near-surface environment due to biological activity?

Methods Used to Collect and Interpret Data

Sample Collection and Field Measurements

During the eastern Puerto Rico WEBB program, two principal types of samples were collected: grab samples, which were manually collected on a regular basis from riverbanks at well-mixed cross sections near each gage site, and event samples, which were collected by an automated sampler during storm events and retrieved when weather conditions permitted. Conductivity, temperature, pH, and dissolved oxygen (O_2) of grab samples were measured onsite; only conductivity was measured onsite for event samples, because the other field measurements are unstable and thus incorrect if not measured immediately. Depth-integrated samples for suspended sediment were occasionally collected at the same time as a grab sample. All water samples were filtered through 0.2-micrometer (μm) filters as soon as practicable in the laboratory. Sample collection and processing are described in detail in appendix 2.

The automated sampler was programmed to begin sampling when the river rose above a preset stage (appendix 1). Once triggered, all 24 bottles were filled at preset times determined beforehand using representative storm hydrographs. The sampler had to be emptied and restarted manually. Thus, a small storm could prevent the sampling of a subsequent, larger storm and, consequently, trigger levels were gradually raised to ensure sampling of the largest storms. Event samples were a crucial part of the study, because only 20 grab samples were collected in the top 50 percent of runoff, and 2 in the top 10 percent, compared with thousands of event samples. This protocol allowed us to sample several massive storms during the study period, including Hurricane Hortense in September 1996, Hurricane Georges in September 1998, and a powerful upper-level trough in May 2003. Samples from these storms enabled accurate estimation of mass discharge of constituents at high runoff. Owing to the enormous volume of event samples (even after threshold stages were increased), analyses performed on event samples were eventually reduced to stable constituents that are sufficient to assess primary processes (conductivity, $Si(OH)_4$, Cl^-, suspended sediment, and usually DOC and K^+).

Stream Discharge

The characterization of mass balances requires high-resolution discharge data to estimate stream discharge at the moment of sampling. The collection frequency was every 5 minutes for the Río Mameyes and every 15 minutes for the remaining rivers, and time stamps were used to match chemistry samples to discharge (appendix 1). All discharge datasets had gaps, ranging from 30 minutes to several months. Commonly the longest gaps were associated with the loss of a streamgage caused by a huge storm, and the length of the gap

reflects the time needed to rebuild the gage. The procedures for determining sample discharge and estimating missing data are described in appendix 1. Estimated data were not used in determining the relation between concentration and discharge discussed below.

Analytical Procedures

The water-quality analytical program was built around a core suite of chemical measurements: field measurements (temperature, conductivity, pH, and dissolved oxygen), major cations (Na^+, K^+, Mg^{2+}, and Ca^{2+}), nutrients (nitrite (NO_2^-), nitrate (NO_3^-), ammonium ion (NH_4^+), and phosphate ($-PO_4^{3-}$)), major anions (Cl^- and SO_4^{2-}), alkalinity, $Si(OH)_4$, and DOC. Suspended solids were measured from the weight of filtered material per unit volume following drying to 105°Celsius (C). Sample preservation and analysis are described in appendix 2. Alkalinity, temperature, and pH were used to calculate the partial pressure of carbon dioxide, P_{CO_2}, CO_2 saturation, O_2 saturation, and the saturation index for calcite, $SI_{calcite}$, following Stumm and Morgan (1981), in grab samples (appendix 1).

Discharge, Load, Runoff, and Yield

Hydrologic and water-quality data, including several million discharge measurements, thousands of precipitation measurements (from automated rain gages), and almost 10,000 water quality samples were reprocessed for rate calculations as described in appendix 1. Constituent loads were calculated from concentrations by using the computer program LOAD ESTimator (LOADEST; Runkel and others, 2004), which estimates constituent loads in streams and rivers given a time series of stream discharge, constituent concentration, and additional explanatory variables (typically, seasonal cycles (sine and cosine of time in a one-year cycle), and time). LOADEST assists the user in developing a regression model of constituent load (calibration); the model then is used to estimate loads over a specific time interval (estimation).

The construction of the input data files used by LOADEST (Runkel and others, 2004) from our datasets was automated and required some minor adaptations (appendix 1). First, the shortest time step allowed by LOADEST for the time series of explanatory variables is 1 hour, so discharge data were resampled from 5-minute and 15-minute intervals into 1-hour intervals. Estimated Na^+, K^+, Mg^{2+}, Ca^{2+}, alkalinity, Cl^-, SO_4^{2-}, $Si(OH)_4$, DOC, NO_3^-, NH_4^+, $-PO_4^{3-}$, and suspended solid loads are discussed here; several more parameters (including bedrock-derived Na^+, K^+, Mg^{2+}, and Ca^{2+}, total dissolved silicate bedrock, total dissolved bedrock cations, suspended bedrock, and particulate organic carbon) are discussed in Stallard (2012b). Complete chemistry was more intensely sampled from 1991 through 2000, whereas Cl^-, $Si(OH)_4$, K^+, and suspended solids were sampled intensively through 2004 (table 5 in appendix 1). These changes in sampling intensity means that for most properties LOADEST is primarily being modeled on the first 10 years of data.

LOADEST is fundamentally a regression, and biases produced by the logarithmic transformation of data and non-normality of the fits to the log-transformed data can produce problems (Runkel and others, 2004). For example, alkalinity loads for the Icacos and Guabá watersheds cannot be estimated directly using LOADEST, because at highest discharge values, alkalinity is sometimes negative (acidity). Discharge, seasonal cycles, and time trends are the core explanatory variables in LOADEST. Some samples have real, but aberrant, concentrations caused by phenomena not strictly related to discharge, time, or seasonality. Some of these measurements, as discussed later in this report, were not included in load estimation; one example is high-chloride storms. These samples are summarized in appendix 1, and the effect of the excluded data on yields is discussed below.

The areas of the study watersheds range from 0.114 square kilometers (km^2) to 26.42 km^2, so for interwatershed comparisons we converted discharge and loads to runoff rates (discharge/area) and yields (constituent load/area). Average yields were totaled, and average concentrations were calculated from average yield divided by average runoff (table 1). Data are presented both in mass units and molecular units for comparison with other datasets. Concentration data (top two sections, table 1) allow for comparison of water quality, whereas yields (bottom two sections, table 1) allow comparison of rates at which constituents are being released into the rivers.

The forested rivers are wetter (mean annual runoff 2,750 to 3,760 millimeters per year (mm yr^{-1}) than the developed watersheds (970 to 1,620 mm yr^{-1}; table 1), so to compare samples from equivalent parts of hydrographs, runoff rates were ranked by their overall contribution to annual runoff. All water-quality samples were assigned into runoff-rate percentile classes, similar to the approach used by the U.S. Geological Survey WaterWatch website (*http://water.usgs.gov/waterwatch/*) in monitoring flood and drought conditions throughout the United States. WaterWatch ranks discharge into percentile classes based on the amount of time a river flows in a given discharge range. For this study, however, percentile classes (0–10, greater than (>)10–25, >25–50, >50–75, >75–90, >90–95, >95–99, and >99 percent) are based on runoff (for example, the 10th percentile corresponds to the runoff rate below which 10 percent of the total runoff has been discharged from the watershed; table 2). Rising and falling stage are also distinguished for each sample. The runoff rates and predicted constituent-yield rates for each percentile class of each river were calculated by using all runoff measurements for the 15-year period. Predicted constituent yields and instantaneous runoff were totaled for each percentile class, and a discharge-weighted average concentration for each percentile class was then calculated by dividing total yield for each constituent by total runoff within that class (table 3). When base flow is referred to in this text, it represents the samples in the 0-to-10 percent range. The cumulative fraction of constituent yield that corresponds to each percentile class was also calculated (table 4).

Table 1. Average constituent concentrations and yields of four watersheds during the study period (1991–2005), eastern Puerto Rico.

[DOC, dissolved organic carbon; SSOL, suspended solids; mm yr^{-1}, millimeters per year; –N, as nitrogen; –P, as phosphorus; -- not applicable]

Average reporting units and watershed	Years of data	Average runoff (mm yr^{-1})	Na^+	K^+	Mg^{2+}	Ca^{2+}	SiO_2	Alkalinity[1]	Cl^-	SO_4^{2-}	DOC	NO_3^-–N	NH_4^+–N	PO_4^{3-}–P	SSOL
Mass concentration (milligrams per liter)															
Canóvanas	15	970	9.82	1.28	4.81	11.49	10.29	10.90	11.76	4.32	3.86	0.625	0.051	0.012	435
Cayaguás	15	1,620	9.55	2.13	2.05	6.17	11.48	6.95	8.99	4.63	2.88	0.705	0.038	0.018	1,302
Mameyes	15	2,750	5.30	0.72	1.54	6.39	7.54	4.67	6.97	2.95	2.50	0.133	0.010	0.005	118
Icacos	15	3,760	4.40	0.59	0.95	2.76	6.26	2.73	5.42	1.37	2.63	0.163	0.013	0.001	560
Guabá	10	3,630	4.42	0.62	0.78	2.02	6.40	1.98	6.47	1.20	2.02	0.159	0.011	0.002	569
Mole concentration (micromoles per liter)															
Canóvanas	15	970	427	33	198	287	366	908	332	45	321	45	3.7	0.40	--
Cayaguás	15	1,620	415	54	84	154	409	579	254	48	240	50	2.7	0.58	--
Mameyes	15	2,750	230	18	63	159	268	389	197	31	208	9	0.7	0.15	--
Icacos	15	3,760	192	15	39	69	223	227	153	14	219	12	1.0	0.05	--
Guabá	10	3,630	192	16	32	51	228	165	182	12	169	11	0.8	0.05	--
Mass yield (metric tons per square kilometer per year)															
Canóvanas	15	970	9.6	1.2	4.7	11.2	10.0	10.6	11.5	4.2	3.8	0.61	0.05	0.012	424
Cayaguás	15	1,620	15.5	3.4	3.3	10.0	18.6	11.3	14.6	7.5	4.7	1.14	0.06	0.029	2,109
Mameyes	15	2,750	14.6	2.0	4.2	17.6	20.7	12.9	19.2	8.1	6.9	0.37	0.03	0.013	325
Icacos	15	3,760	16.9	2.3	3.6	10.6	24.0	10.4	20.7	5.2	10.0	0.62	0.05	0.006	2,144
Guabá	10	3,630	15.1	2.1	2.7	6.9	21.9	6.8	22.1	4.1	6.9	0.54	0.04	0.006	1,944
Mole yield (kilomoles per square kilometer per year)															
Canóvanas	15	970	417	32	193	280	357	886	324	44	313	44	3.6	0.39	--
Cayaguás	15	1,620	672	88	136	249	662	937	411	78	389	82	4.4	0.94	--
Mameyes	15	2,750	634	51	174	439	739	1,071	541	85	573	26	2.1	0.41	--
Icacos	15	3,760	733	58	150	264	853	869	585	54	837	45	3.7	0.18	--
Guabá	10	3,630	657	54	109	173	779	562	623	43	576	39	2.6	0.18	--

[1]Alkalinity mass concentration units are milligrams carbon per liter; alkalinity mole concentration units are microequivalents per liter; alkalinity mass-yield units are metric tons carbon per square kilometer per year; alkalinity mole-yield units are kiloequivalents per square kilometer per year.

Table 2. Runoff rates for Water, Energy, and Biogeochemical Budgets program rivers during the study period (1991–2005) at certain thresholds.

River	Minimum runoff	Percentile of annual runoff volume							Maximum runoff
		10	25	50	75	90	95	99	
	Runoff rate (millimeters per hour)								
Canóvanas	0.009	0.041	0.083	0.246	1.43	8.10	20.3	43.1	69.0
Cayaguás	0.020	0.073	0.114	0.270	1.79	7.76	17.9	40.6	54.8
Mameyes	0.024	0.141	0.222	0.457	1.49	4.95	11.0	43.3	89.8
Icacos	0.059	0.203	0.290	0.566	2.14	7.51	14.0	36.4	86.0
Guabá	0.036	0.196	0.287	0.477	1.84	10.92	25.5	63.7	118.8

For each constituent for each river the relation between log(concentration) and log(runoff rate) was determined using regressions on the primary data following Godsey and others (2009). In each case, a linear regression,

$$\log(C) = C_0 + C_1 \bullet \log(R)$$

was compared to a quadratic regression,

$$\log(C) = C_0 + C_1 \bullet \log(R) + C_2 \bullet \log(R)^2,$$

where C_0, C_1, and C_2 are regression constants. A t-test (Bevington and Robinson, 2003) was used to determine whether the slope of the linear regression, C_1, was statistically different, with 95 percent confidence, from a zero slope (the chemostat condition). An F-test (Bevington and Robinson, 2003) was used to determine whether the quadratic regression significantly reduced the residual error, with 95 percent confidence, compared to the linear regression or to no regression. The most statistically significant regressions are indicated in table 4. Also, for reference, the constant-input and chemostat conditions of Godsey and others (2009) are provided.

The amount of variance explained by the simple regressions, as compared to LOADEST, was also compared (table 4). In all cases, LOADEST explains more of the data variance than do the simple regressions. An F-test was used to evaluate the likelihood that the LOADEST model results offer a statistically more significant explanation of the dataset.

Water Quality of Eastern Puerto Rico WEBB Project Watersheds

The water quality data produced during the first 15 years of the eastern Puerto Rico WEBB project are available from the U.S. Geological Survey's National Water Information System website (*http://waterdata.usgs.gov/nwis)*. The results are summarized and interpreted here. Suspended-sediment yield differed greatly among the study watersheds (table 1). Yields were larger than 1,900 metric tons per square kilometer per year (t km^{-2} yr^{-1}) in granitic watersheds (Icacos, Guabá, and Cayaguás), and about one-sixth this value from volcaniclastic watersheds (Mameyes and Canóvanas), independent of land cover and climate (the developed watersheds, Canóvanas and Cayaguás, are drier, having both less rainfall and runoff (Murphy and Stallard, 2012)). However, dissolved constituent yields were not very different among watersheds of different geology. Yields of nonbioactive constituents derived largely from bedrock weathering (Ca^{2+}, alkalinity, $Si(OH)_4$), from seasalt (Cl^-), or from a mix of the two sources (Na^+, Mg^{2+} and SO_4^{2-}) differed by a factor of less than 2 among all watersheds, showing little relation to land cover, annual runoff, or bedrock type. Nutrient yields were consistently greater in the developed watersheds, despite their lesser runoff. Most dissolved constituents have clearly defined runoff-concentration relations; however, the field measurements and several nutrients (nitrate, ammonium ion, and phosphate) do not.

Runoff Percentile Classes, Concentration, and Yield

Percentile classes correspond to equivalent parts of the hydrograph for each river, so comparing constituent yield per percentile class of runoff provides a means of comparing the relation between runoff and constituent concentration among all watersheds. The percentage of time that runoff is below each threshold in each watershed and the percentage of constituent yield discharged below that threshold are shown in table 4. Constituents are sorted by decreasing yields at 50 percent of runoff. The constituents are therefore ordered from those that are most diluted at higher discharge to those that become most concentrated. For reference, the constant-rate input (equivalent to time) and the "chemostat" input (equivalent to runoff) of Godsey and others (2009) are indicated.

Eighty-five percent of the time, the runoff in the WEBB rivers was less than half of the maximum runoff rate (the constant-rate line in table 4). For example, in the Canóvanas watershed, the lowest 50 percent of runoff rates were recorded, on average, 93.8 percent of the time, or about 342 days' worth of time in a year. The lowest 75 percent of runoff rates were recorded 99.4 percent of the time, or about 363 days' worth of time in a year. In other words, the highest 25th percentile of runoff rates was reached only for 2 days' worth of time in a year, during large storms. The lowest 50 percent of runoff rates corresponds to the export of 70.8 percent of Ca^{2+} from the Canóvanas watershed, but only 38.8 percent of DOC and 4.5 percent of suspended sediment. The lowest 90 percent of runoff rates exports only 53.7 percent of suspended sediment; that is, almost half of suspended sediment is exported when runoff exceeds the 90th percentile, during storm events that total less than 1 day per year.

Table 3. Discharge-weighted average concentrations of each percentile class estimated by using LOADEST and hourly discharge.

[DOC, dissolved organic carbon; mm h^{-1}, millimeters per hour; m^3 s^{-1}, cubic meters per second; mg L^{-1}, milligrams per liter; µS cm^{-1}, microsiemens per centimeter; µmol L^{-1}, micromoles per liter; µeq L^{-1}, microequivalents per liter; ppmv, parts per million by volume]

Sample percentile class (percent)	Runoff rate (mm h^{-1})	Discharge (m^3 s^{-1})	Suspended sediment (mg L^{-1})	Conductivity (µS cm^{-1})	pH[1]	Na^+ (µmol L^{-1})	K^+ (µmol L^{-1})	Mg^{2+} (µmol L^{-1})	Ca^{2+} (µmol L^{-1})	$Si(OH)_4$ (µmol L^{-1})	Alkalinity (µEq L^{-1})	Cl^- (µmol L^{-1})	SO_4^{2-} (µmol L^{-1})	DOC (µmol L^{-1})	NO_3^- (µmol L^{-1})	NH_4^+ (µmol L^{-1})	$-PO_4^{3-}$ (µmol L^{-1})	Partial pressure of CO_2 (ppmv)	Saturation index of calcite
Canóvanas																			
0–10	0.021	0.149	9.8	223	8.34	713	20.6	386	564	580	2,044	459	53.8	164	11.1	2.4	0.36	565	0.21
>10–25	0.061	0.430	29.6	173	8.20	573	25.7	284	422	488	1,450	416	51.3	232	24.3	2.3	0.45	565	–0.17
>25–50	0.158	1.12	87.7	138	8.06	473	30.5	214	318	410	1,035	368	47.8	299	45.3	2.4	0.46	565	–0.55
>50–75	0.765	5.42	448	96	7.82	351	38.5	139	197	292	586	291	42.9	414	66.3	2.9	0.46	556	–1.20
>75–90	4.49	31.8	1,242	66.9	7.69	258	41.3	91.3	118	206	349	208	35.0	420	62.1	5.6	0.28	458	–1.75
>90–95	15.3	108	1,792	53.5	7.67	214	39.6	71.4	83.9	159	282	165	29.9	374	37.2	10.8	0.17	383	–1.98
>95–99	32.0	227	2,042	47.3	7.67	193	37.4	62.2	68.3	138	265	138	26.3	323	25.2	16.1	0.12	366	–2.09
>99–100	59.2	419	2,152	42.9	7.65	179	33.8	55.4	57.0	119	254	122	24.1	266	13.8	21.5	0.07	366	–2.20
Cayaguás																			
0–10	0.041	0.301	13.2	169	7.65	883	36.6	167	312	680	1,395	347	48.7	123	28.9	1.0	1.10	1,932	–0.84
>10–25	0.095	0.698	41.2	135	7.51	651	45.6	137	253	592	997	321	51.4	168	43.4	1.7	0.92	1,932	–1.20
>25–50	0.195	1.43	139.2	106	7.34	499	54.0	103	189	493	669	296	52.4	221	52.4	2.4	0.67	1,932	–1.64
>50–75	0.860	6.31	1,063	65.9	6.94	307	65.3	51.7	91.8	315	250	233	49.8	312	61.0	3.7	0.36	1,831	–2.73
>75–90	4.35	32.0	3,441	41.8	6.66	193	63.3	25.7	44.0	186	80	158	42.2	324	58.1	4.0	0.24	1,117	–3.79
>90–95	12.1	89.0	5,697	31.6	6.70	148	54.7	17.3	29.0	127	48	119	36.0	278	42.8	3.4	0.21	618	–4.14
>95–99	26.2	192	7,184	24.6	6.82	119	46.2	12.1	20.0	91.5	38	93.4	30.5	231	25.9	2.6	0.19	372	–4.28
>99–100	41.0	301	6,984	21.4	6.77	106	42.2	9.9	16.2	78.9	33	80.9	27.7	212	19.7	2.2	0.17	366	–4.46
Mameyes																			
0–10	0.068	0.339	1.6	110	7.97	379	19.1	114	320	571	914	252	43.5	80	7.0	1.0	0.36	617	–0.67
>10–25	0.179	0.884	4.8	82	7.80	295	18.7	85.1	224	372	615	227	36.7	133	7.3	0.7	0.21	617	–1.13
>25–50	0.324	1.61	12.8	68.4	7.68	254	18.4	69.7	176	296	469	209	32.9	178	8.0	0.6	0.16	617	–1.45
>50–75	0.887	4.39	56.4	51.6	7.49	202	18.1	51.0	120	205	297	184	27.8	245	9.7	0.6	0.10	608	–1.98
>75–90	2.81	13.9	217	38.5	7.32	164	18.0	35.6	77.7	139	173	157	23.0	308	12.4	0.7	0.07	526	–2.56
>90–95	7.26	36.0	567	30.9	7.18	142	18.5	26.0	53.3	98.4	106	135	19.3	358	15.2	1.1	0.06	449	–3.05
>95–99	21.2	105	1,275	25.0	7.02	123	19.1	18.6	35.6	69.8	61	114	16.1	347	20.1	1.8	0.06	374	–3.62
>99–100	45.6	226	2,054	22.3	6.87	112	19.5	15.1	27.5	53.6	42	104	14.4	320	22.8	2.6	0.06	366	–4.04

Table 3. Discharge-weighted average concentrations of each percentile class estimated by using LOADEST and hourly discharge.—Continued

[DOC, dissolved organic carbon; mm h^{-1}, millimeters per hour; m^3 s^{-1}, cubic meters per second; mg L^{-1}, milligrams per liter; µS cm^{-1}, microsiemens per centimeter; µmol L^{-1}, micromoles per liter; µeq L^{-1}, microequivalents per liter; ppmv, parts per million by volume]

Sample percentile class (percent)	Runoff rate (mm h^{-1})	Discharge (m^3 s^{-1})	Suspended sediment (mg L^{-1})	Conductivity (µS cm^{-1})	pH[1]	Na^+ (µmol L^{-1})	K^+ (µmol L^{-1})	Mg^{2+} (µmol L^{-1})	Ca^{2+} (µmol L^{-1})	$Si(OH)_4$ (µmol L^{-1})	Alkalinity (µEq L^{-1})	Cl^- (µmol L^{-1})	SO_4^{2-} (µmol L^{-1})	DOC (µmol L^{-1})	NO_3^- (µmol L^{-1})	NH_4^+ (µmol L^{-1})	$-PO_4^{3-}$ (µmol L^{-1})	Partial pressure of CO_2 (ppmv)	Saturation index of calcite
Icacos																			
0–10	0.115	0.104	3.7	61.5	6.83	283	16.4	61.7	118	475	426	191	12.2	75	14.6	1.0	0.05	4,053	–2.50
>10–25	0.252	0.228	10.9	52.9	6.72	243	16.4	53.0	97.1	331	332	182	13.6	125	13.5	1.0	0.05	4,053	–2.79
>25–50	0.429	0.389	27.7	45.7	6.62	213	16.2	45.3	80.2	256	265	167	14.3	186	12.3	1.0	0.05	4,053	–3.06
>50–75	1.197	1.08	168.7	35.8	6.46	176	15.5	33.3	55.0	154	165	147	15.5	299	11.1	1.0	0.05	3,677	–3.58
>75–90	3.96	3.59	832	25.6	6.35	135	13.9	21.3	32.5	86.5	79	118	15.7	368	10.0	0.9	0.05	2,293	–4.21
>90–95	9.04	8.18	2,105	20.1	6.31	110	12.6	15.1	21.7	59.1	41	98.7	15.3	349	9.6	0.9	0.05	1,328	–4.70
>95–99	20.8	18.8	5,637	15.6	6.38	89.9	11.1	10.2	13.9	39.8	17	80.6	14.4	285	9.1	0.9	0.05	475	–5.19
>99–100	51.6	46.7	21,372	12.8	5.46	67.6	8.8	6.3	8.0	25.8	–2	61.9	12.8	149	11.3	0.9	0.05	366	–7.37
Guabá																			
0–10	0.104	0.003	5.6	57.0	6.87	295	12.8	51.3	87.4	443	321	224	11.8	79	12.7	0.5	0.05	2,765	–2.70
>10–25	0.250	0.008	16.8	48.7	6.74	257	15.7	40.6	67.1	313	235	212	11.8	120	12.1	0.6	0.05	2,765	–3.08
>25–50	0.383	0.012	37.2	44.5	6.66	237	16.9	35.6	57.0	264	194	203	11.9	142	12.2	0.6	0.06	2,765	–3.30
>50–75	0.950	0.030	198	37.0	6.50	202	18.3	27.2	41.4	171	130	181	12.5	205	11.4	0.8	0.06	2,640	–3.76
>75–90	4.48	0.142	1,460	25.2	6.41	142	15.7	17.2	23.5	83.1	59	130	14.1	265	10.1	1.1	0.05	1,473	–4.42
>90–95	14.48	0.459	3,307	18.9	6.51	110	12.1	12.8	15.9	50.4	30	96.9	15.6	264	9.0	1.3	0.05	604	–4.76
>95–99	33.1	1.05	4,943	14.3	6.46	86.4	9.2	9.5	11.3	33.7	16	69.6	16.1	259	7.8	1.5	0.04	366	–5.22
>99–100	68.6	2.17	6,866	11.1	6.18	69.5	6.9	7.0	7.9	25.0	8	48.6	16.3	223	7.3	1.6	0.03	366	–5.93

[1]pH is calculated from CO_2 vapor pressure. Grab samples collected at high runoff rates on the Icacos also indicate equilibration with the atmosphere during high-flow conditions. All rivers were assumed to change from their low-runoff-rate averages to atmospheric equilibrium at high runoff rates. The transition from low runoff rate to high runoff rate values of P_{CO_2} was assigned to the 3 to 20 mm hr^{-1} interval for which the slope of the DOC-runoff relation goes from positive to negative, indicating shallow flowpaths.

Table 4. Percentage of constituent discharged compared with percentage of water discharged (estimated by using LOADEST) and comparisons with regressions of log(concentration) to log(runoff rate).

[Constant rate, a hypothetical constituent introduced at a constant rate, independent of runoff rate; chemostat, a hypothetical constituent introduced at a rate that is proportional to runoff rate. Bold column, 50 percent runoff; bold rows, constant-rate and chemostat models; C_1, linear regression coefficient relating log(concentration) to log(runoff); C_2, quadratic coefficient, if quadratic regression is statistically more significant; [], values are not statistically different from zero; F-test, likelihood that the best LOADEST model offers statistically more significant explanation of data set; DOC, dissolved organic carbon; -- not applicable]

Constituent	Percentile of annual runoff volume, in percent estimated using LOADEST							Regression on all measurements		Data count	Regression order	Percent variance explained	Best LOADEST model[1]	Percent variance explained	F-test LOADEST choice
	10	25	50	75	90	95	99								
	Yield of each constituent (percent)							C_1	C_2						
Canóvanas															
Constant rate	**42.8**	**73.2**	**93.8**	**99.4**	**99.9**	**100.0**	**100.0**	**–1**	--	--	--	--	--	--	--
Calcium	18.8	41.6	**70.8**	90.4	97.3	98.9	99.8	–0.29	--	140	1	82	1	82	--
Magnesium	18.5	40.8	**69.3**	89.1	96.6	98.5	99.8	–0.26	--	140	1	82	2	82	--
Silica	15.4	35.8	**64.9**	86.8	95.9	98.2	99.7	–0.20	--	767	1	61	9	62	--
Sodium	15.6	35.9	**63.9**	85.9	95.5	98.0	99.7	–0.18	--	140	1	80	4	81	--
Chloride	13.9	33.1	**61.5**	85.2	95.5	98.0	99.7	–0.16	--	739	1	51	9	54	76
Sulfate	12.1	29.5	**56.5**	81.4	93.8	97.2	99.6	–0.09	--	145	1	61	9	69	78
Phosphate	9.1	25.7	**55.9**	84.6	96.3	98.7	99.8	[–0.03]	--	133	1	0	8	44	100
Chemostat	**10.0**	**25.0**	**50.0**	**75.0**	**90.0**	**95.0**	**99.0**	**0**	--	--	--	--	--	--	--
Potassium	6.6	18.2	**41.3**	69.4	88.4	94.6	99.2	0.12	--	451	1	39	9	49	99
DOC	5.4	16.0	**38.8**	69.1	89.2	95.2	99.3	0.10	–0.12	315	2	56	8	59	--
Nitrate	2.8	10.6	**34.7**	70.2	92.7	97.3	99.7	0.05	–0.27	145	2	67	9	75	--
Ammonium ion	6.0	14.9	**30.4**	48.0	66.6	79.7	96.0	0.26	--	85	1	21	6	42	100
Sediment	0.2	1.0	**4.5**	20.4	53.7	75.0	95.8	0.74	–0.24	1,337	2	73	8	75	--
Cayaguás															
Constant rate	**33.9**	**63.7**	**91.1**	**99.0**	**99.9**	**100.0**	**100.0**	**–1**	--	--	--	--	--	--	--
Calcium	18.8	43.3	**75.7**	93.3	98.3	99.3	99.9	–0.42	--	105	1	87	4	89	--
Magnesium	18.5	42.7	**74.9**	92.9	98.2	99.2	99.9	–0.40	--	105	1	88	4	89	--
Phosphate	17.8	41.5	**72.3**	89.9	96.5	98.4	99.7	–0.27	--	91	1	38	6	43	--
Sodium	17.3	39.7	**70.7**	90.3	97.0	98.7	99.8	–0.31	--	105	1	93	9	94	--
Silica	15.6	37.2	**68.2**	89.6	97.2	98.8	99.8	–0.31	--	774	1	87	9	88	--
Chloride	13.1	32.0	**61.4**	85.7	95.7	98.1	99.7	–0.20	--	785	1	78	9	85	89
Sulfate	10.2	26.1	**53.0**	79.3	93.0	96.8	99.4	–0.08	--	109	1	43	2	56	92
Chemostat	**10.0**	**25.0**	**50.0**	**75.0**	**90.0**	**95.0**	**99.0**	**0**	--	--	--	--	--	--	--
Nitrate	6.5	19.3	**44.1**	73.7	92.5	97.1	99.6	[–0.02]	--	105	1	1	9	31	100
Potassium	7.1	19.5	**43.5**	72.6	90.5	95.7	99.2	0.04	–0.10	395	2	42	8	44	--
DOC	5.8	16.3	**38.1**	68.7	89.0	94.9	99.1	0.12	–0.14	98	2	68	8	70	--
Ammonium ion	4.4	13.5	**34.2**	66.1	88.5	94.9	99.2	0.13	--	62	1	9	2	19	100
Sediment	0.1	0.5	**2.5**	16.8	50.5	72.4	94.1	1.03	–0.34	991	2	89	8	90	--
Mameyes															
Constant rate	**30.8**	**58.7**	**86.0**	**97.5**	**99.7**	**99.9**	**100.0**	**–1**	--	--	--	--	--	--	--
Phosphate	19.3	41.2	**69.1**	88.2	96.0	98.1	99.6	–0.35	--	141	1	42	2	45	--
Calcium	17.6	39.1	**68.1**	88.9	97.0	98.8	99.8	–0.37	--	177	1	89	4	89	--
Silica	17.2	38.4	**67.3**	88.2	96.7	98.7	99.8	–0.34	--	1,165	1	59	9	62	86
Magnesium	16.1	36.7	**65.3**	87.1	96.3	98.5	99.8	–0.29	--	177	1	85	4	86	--
Sodium	13.6	32.2	**60.1**	83.8	94.9	97.8	99.6	–0.19	--	177	1	86	8	88	--
Sulfate	13.2	31.3	**58.7**	82.3	94.1	97.3	99.5	–0.17	--	179	1	86	7	87	--

Table 4. Percentage of constituent discharged compared with percentage of water discharged (estimated by using LOADEST) and comparisons with regressions of log(concentration) to log(runoff rate).—Continued

[Constant rate, a hypothetical constituent introduced at a constant rate, independent of runoff rate; chemostat, a hypothetical constituent introduced at a rate that is proportional to runoff rate. bold column, 50 percent runoff; bold rows, constant-rate and chemostat models; C_1, linear regression coefficient relating log(concentration) to log(runoff); C_2, quadratic coefficient, if quadratic regression is statistically more significant; [], values are not statistically different from zero; F-test, likelihood that the best LOADEST model offers statistically more significant explanation of data set; DOC, dissolved organic carbon; -- not applicable]

Constituent	Percentile of annual runoff volume, in percent estimated using LOADEST							Regression on all measurements		Data count	Regression order	Percent variance explained	Best LOADEST model[1]	Percent variance explained	F-test LOADEST choice
	10	25	50	75	90	95	99								
	Yield of each constituent (percent)							C_1	C_2						
Mameyes—Continued															
Chloride	12.4	29.8	**56.9**	81.1	93.5	97.1	99.5	–0.14	--	1,134	1	33	9	39	100
Potassium	10.3	25.5	**50.5**	75.1	89.8	94.8	98.9	[–0.00]	--	581	1	0	8	5	100
Chemostat	**10.0**	**25.0**	**50.0**	**75.0**	**90.0**	**95.0**	**99.0**	**0**	**--**	**--**	**--**	**--**	**--**	**--**	**--**
Ammonium ion	10.1	23.0	**42.0**	60.4	74.4	82.2	94.0	[–0.07]	--	57	1	1	2	10	100
Nitrate	7.2	18.7	**39.3**	63.5	82.1	89.6	97.5	0.24	--	178	1	44	9	54	90
DOC	4.8	14.4	**34.9**	62.4	83.3	91.6	98.4	0.32	–0.18	164	2	82	9	84	--
Sediment	0.1	0.6	**2.6**	10.5	30.9	50.1	84.0	1.18	--	1,248	1	77	8	79	--
Icacos															
Constant rate	**28.0**	**56.3**	**85.6**	**97.6**	**99.6**	**99.9**	**100.0**	**–1**	**--**	**--**	**--**	**--**	**--**	**--**	**--**
Silica	18.9	42.2	**72.4**	91.5	97.7	99.1	99.9	–0.54	--	1,074	1	81	4	82	--
Calcium	16.1	37.8	**67.6**	89.2	97.1	98.9	99.8	–0.42	--	238	1	86	6	88	--
Magnesium	15.0	35.7	**65.1**	87.6	96.5	98.6	99.8	–0.35	--	237	1	85	6	88	--
Sodium	12.8	31.1	**58.9**	83.0	94.5	97.6	99.6	–0.19	--	237	1	71	8	78	--
Chloride	12.3	30.0	**57.6**	82.3	94.3	97.5	99.6	–0.16	--	1,104	1	38	9	52	100
Nitrate	11.2	28.3	**54.8**	79.1	92.0	96.1	99.1	–0.13	--	235	1	26	9	31	90
Ammonium ion	12.0	28.5	**53.5**	75.9	89.3	94.1	98.6	[–0.02]	--	136	1	0	1	0	--
Potassium	10.7	26.7	**53.1**	78.5	92.3	96.5	99.4	–0.07	--	607	1	17	9	24	100
Chemostat	**10.0**	**25.0**	**50.0**	**75.0**	**90.0**	**95.0**	**99.0**	**0**	**--**	**--**	**--**	**--**	**--**	**--**	**--**
Phosphate	9.8	24.6	**49.4**	74.4	89.7	94.8	99.0	[0.01]	--	196	1	0	1	0	100
Sulfate	8.2	21.7	**46.2**	73.6	90.5	95.6	99.3	0.03	--	238	1	6	6	20	100
DOC	4.0	11.8	**30.8**	61.3	85.8	93.7	99.2	0.44	–0.32	279	2	80	9	81	--
Sediment	0.1	0.2	**1.0**	5.0	19.9	35.2	67.1	1.41	--	1,408	1	89	9	91	--
Guabá															
Constant rate	**28.5**	**54.9**	**83.5**	**97.9**	**99.8**	**99.9**	**100.0**	**-1**	**--**	**--**	**--**	**--**	**--**	**--**	**--**
Silica	19.0	41.2	**71.1**	92.0	98.0	99.2	99.9	–0.52	--	604	1	93	9	94	--
Calcium	16.8	37.8	**67.1**	89.5	97.2	98.9	99.8	–0.34	--	160	1	88	9	90	--
Magnesium	15.4	35.4	**64.3**	87.5	96.5	98.6	99.8	–0.28	--	158	1	84	9	88	--
Sodium	14.0	33.0	**61.2**	85.3	95.5	98.0	99.7	–0.21	--	158	1	81	9	87	--
Chloride	13.0	31.1	**59.1**	84.1	95.2	98.0	99.7	–0.20	--	640	1	60	9	70	98
Nitrate	11.0	26.9	**53.5**	79.0	92.6	96.6	99.4	–0.07	--	156	1	9	7	18	100
Potassium	10.4	26.1	**52.4**	78.3	92.2	96.3	99.3	0.03	–0.16	324	2	39	9	45	89
Chemostat	**10.0**	**25.0**	**50.0**	**75.0**	**90.0**	**95.0**	**99.0**	**0**	**--**	**--**	**--**	**--**	**--**	**--**	**--**
Phosphate	8.9	23.4	**49.1**	76.3	92.0	96.5	99.4	[–0.02]	--	112	1	2	2	4	100
Sulfate	9.4	23.5	**47.0**	71.3	87.6	93.7	98.8	0.06	--	155	1	35	7	59	100
Ammonium ion	7.0	18.4	**39.1**	62.8	82.3	90.4	98.0	0.17	--	60	1	18	1	18	--
DOC	5.1	15.0	**35.0**	62.0	84.8	92.6	98.7	0.35	–0.24	120	2	65	9	73	--
Sediment	0.1	0.4	**1.6**	6.8	36.1	62.2	91.8	1.25	--	802	1	86	8	89	--

[1]For explanation of model number, see Runkel and others, 2004, their table 7.

The increase in percentage yield of constituents listed in table 4 parallels the increase in the value of the linear regression coefficient (or slope), C_1. The constituents with negative slopes are bedrock-weathering derived, seasalt derived, or a mix of the two ($Si(OH)_4$, Ca^{2+}, Mg^{2+}, Na^{2+}, and Cl^-). Although the order varies slightly among rivers, the constituents that are most dominantly of bedrock origin, $Si(OH)_4$, Ca^{2+}, and Mg^{2+}, produce more negative slopes than Na^{2+}, which has a large seasalt contribution, and Cl^-, nearly all of which is derived from seasalt. Dissolved organic carbon and suspended sediment always have a positive slope, consistent with surface flow-path inputs. Phosphate has slopes that are either negative or indistinguishable from zero, differing considerably among rivers. All remaining constituents have a mix of slopes that are zero or near zero, close to the slope of the chemostat.

Both LOADEST and simple regression models explained most of the data variance, typically more than 80 percent, in the nonbioactive bedrock-derived constituents ($Si(OH)_4$, Ca^{2+}, Mg^{2+}, Na^{2+}, and Cl^-; table 4). The models generally explained less than half the variance of bioactive constituents (K^+, NO_3^-, NH_4^+, and $-PO_4^{3-}$). The LOADEST model, as compared to simple regressions, significantly improved the explanation of variance for the bioactive constituents, presumably by introducing the influence of seasonality and temporal trends (LOADEST models 3–9). Ammonium ion was modeled poorly in most watersheds. Phosphate was not well modeled in the Icacos and Guabá watersheds, whereas K^+ was not well modeled in the Mameyes watershed. These results parallel similar models by Peters and others (2006) in a comparison of the Río Icacos with the four other Puerto Rico WEBB sites using the first years (1991–1997) of the present dataset. They noted that discharge variations and seasonality explained most of the variance in log(concentration) of alkalinity, Ca^{2+}, Mg^{2+}, Na^+, Cl^-, and $Si(OH)_4$, but less than half of the variance of K^+, NO_3^-, and SO_4^{2-}; SO_4^{2-} concentration increased with discharge.

Water-Quality Constituents

The concentration-runoff relations for various constituents (table 3) are consistent with major processes that deliver the constituents to the river—bedrock weathering, seasalt deposition, and biological activity. These relations are reviewed here. Field measurements are presented first, followed by chemical constituents, which are grouped by the major processes that regulate them.

Field Measurements

Water temperature ranges of the rivers were quite narrow (fig. 3), as air temperatures in Puerto Rico do not vary substantially year round. Generally, as runoff increases, temperature decreases. The forested watersheds (Icacos, Guabá, and Mameyes) typically had water temperature values between 18 and 25°C. The developed watersheds (Canóvanas and Cayaguás) generally had higher water temperatures—between 22 and 30°C—because they are located at lower elevations (and hence air temperatures are higher), have less water in streams, and have less riparian vegetation to shade stream channels (see cover photograph).

Dissolved oxygen concentrations of the study rivers were usually close to saturation or slightly undersaturated (fig. 3). Some samples from the Canóvanas watershed were supersaturated; this state is probably due to photosynthesis by aquatic vegetation, which produces oxygen and consumes carbon dioxide during daylight hours (when grab samples were collected). Respiration and decomposition, which continue 24 hours a day, consume oxygen and produce carbon dioxide; therefore, O_2 levels are likely lower at night. The effects of photosynthesis and its relation to carbonate dynamics in the streams are further discussed later in section Alkalinity, Carbon Dioxide, and Calcite Saturation of this chapter.

The pH values of study rivers were typically circumneutral, between 6 and 8. Generally, pH of the study rivers decreases with increasing runoff (fig. 3). The granitic watersheds had the lowest pH values; the forested watersheds (Icacos and Guabá) were of lower pH than the developed watershed (Cayaguás). Highest pH values, as much as 9, were observed in the developed, volcaniclastic Canóvanas. These high pH values are likely related to both the higher alkalinity of the Río Canóvanas (discussed in section Alkalinity, Carbon Dioxide, and Calcite Saturation of this chapter) and to sampling times. Grab samples were always collected during the day, when photosynthesis produces oxygen and consumes carbon dioxide, leading to an increase in pH. Therefore, water likely was sampled when pH values were at a maximum for the day.

Conductivity values, which are affected by all dissolved ions regardless of source, ranged from about 10 to 300 microsiemens per centimeter ($\mu S\ cm^{-1}$). Values were generally lowest in the forested watersheds, and values in the granitic watersheds (Icacos and Guabá) were lower than in the volcaniclastic watershed (Mameyes) (fig. 3). Highest conductivity values were observed in the volcaniclastic, developed Canóvanas watershed. This general pattern was repeated for almost all constituents: at a given runoff rate, forested streams were more dilute. In the pH range of the watersheds, conductivity was a conservative property that generally decreased with increasing runoff, as shallower flow paths during storms decrease the concentrations of constituents that dominate conductivity measurements (such as Cl^- and Na^+). High-chloride samples were a notable exception to this trend, as discussed in a later section entitled “Chloride.”

Silica

Dissolved $Si(OH)_4$ is derived primarily from the weathering of silicate minerals in bedrock and soil. Dissolved $Si(OH)_4$ concentrations decreased markedly with increasing runoff in all eastern Puerto Rico WEBB rivers (fig. 4). This decrease is consistent with the concept that an ever-larger portion of water moves through shallower flow paths, and they hence have less

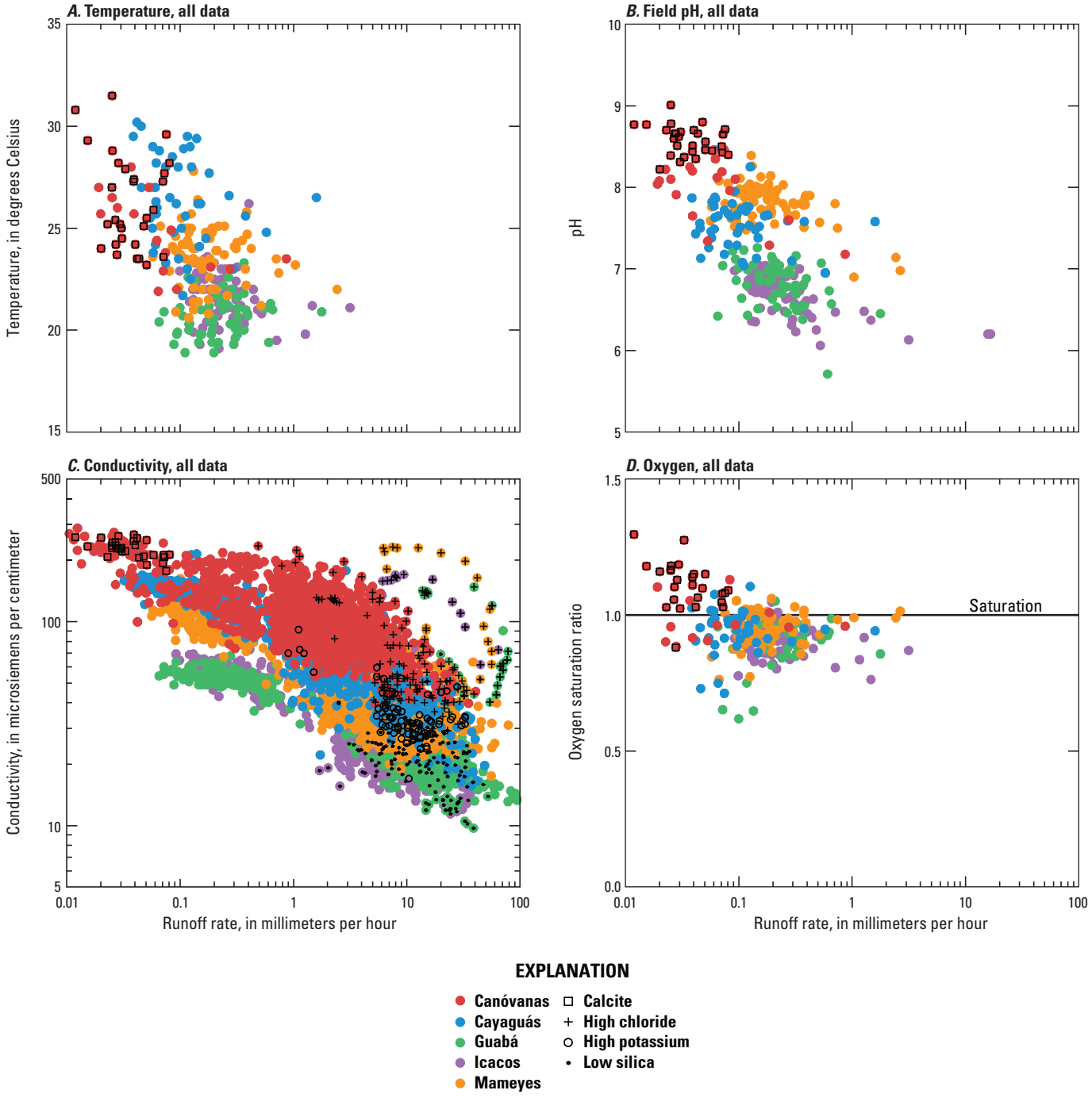

Figure 3. Temperature, pH, conductivity, and dissolved oxygen in the eastern Puerto Rico Water, Energy, and Biogeochemical Budget program rivers, 1991–2005. Additional sample characteristics are indicated with black symbols: calcite, samples supersaturated with respect to calcite; high chloride, samples with exceptionally high chloride concentrations collected during huge storms; high potassium, samples with high potassium but not high chloride; low silica, Icacos and Guabá samples with unusually low silica concentrations for the runoff rate.

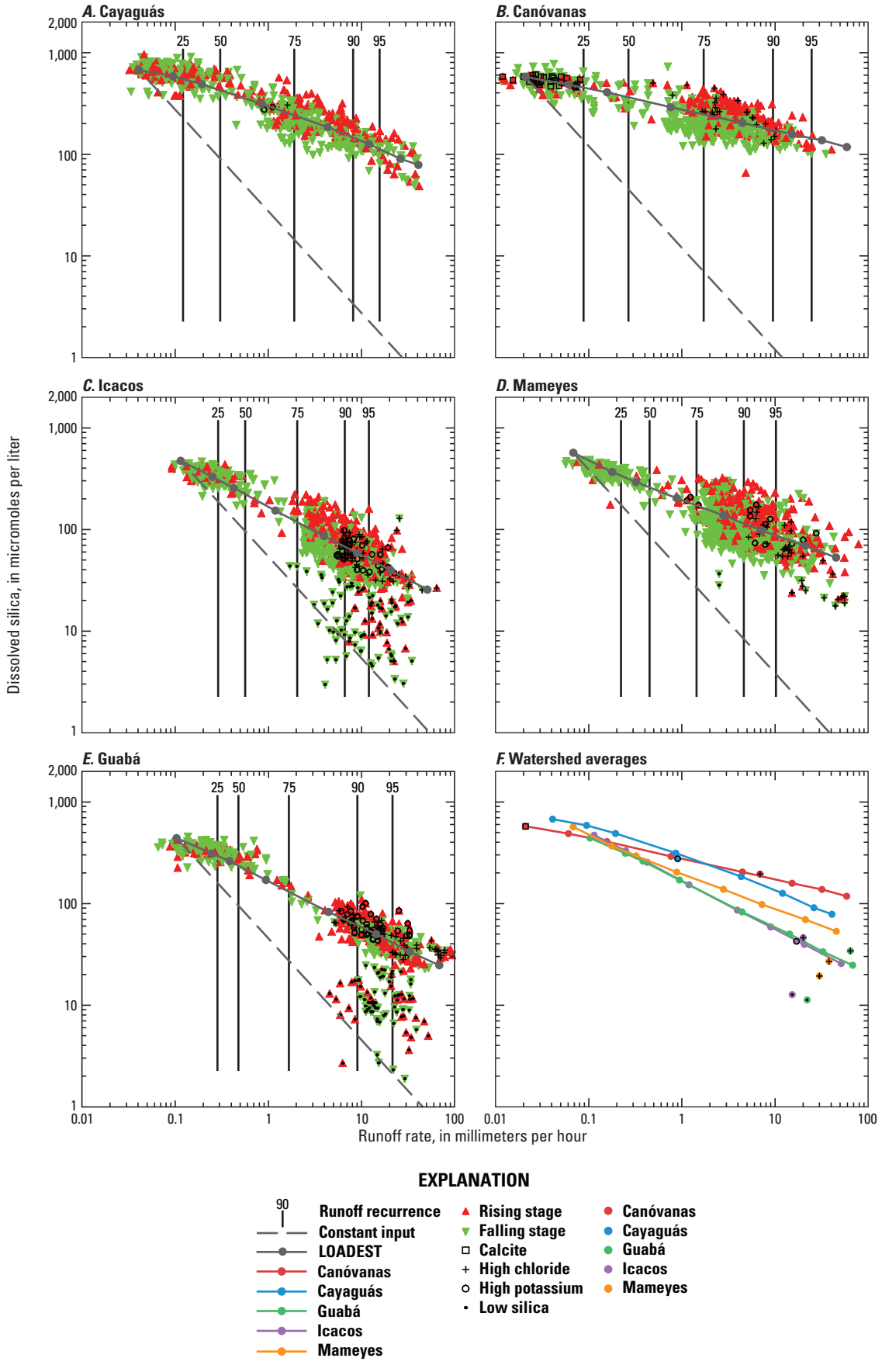
A. Cayaguás
B. Canóvanas
C. Icacos
D. Mameyes
E. Guabá
F. Watershed averages
25
50
75
90
95
2,000
1,000
100
10
1
0.01
0.1
1
10
100
Dissolved silica, in micromoles per liter
Runoff rate, in millimeters per hour
EXPLANATION
Runoff recurrence
Constant input
LOADEST
Canóvanas
Cayaguás
Guabá
Icacos
Mameyes
Rising stage
Falling stage
Calcite
High chloride
High potassium
Low silica
Canóvanas
Cayaguás
Guabá
Icacos
Mameyes

Figure 4 (facing page). Runoff rate–concentration graphs for dissolved silica. Samples in individual rivers are keyed according to runoff percentile class. Averages for runoff percentile class, estimated using LOADEST (see table 3) are indicated in the lower left diagram. Additional sample characteristics are indicated with black symbols: calcite, samples supersaturated with respect to calcite; high chloride, samples with exceptionally high chloride concentrations collected during huge storms; high potassium, samples with high potassium but not high chloride; low silica, Icacos and Guabá samples with unusually low silica concentrations for the runoff rate. The points separated from the watershed-average curves (F) represent the averages of the classes of sample indicated by the superimposed character. These samples are not included in LOADEST models.

contact with deep soil and bedrock, with increasing rainfall and runoff (see Elsenbeer, 2001). Although the Luquillo Mountains receive, on a long-term annual average, about 21±7 t km^{-2} yr^{-1} of Saharan desert dust (Pett-Ridge and others, 2009b), the dust likely does not contribute substantially to dissolved $Si(OH)_4$. More than 85 percent of the dust is composed of aluminosilicate clay minerals (such as illite, kaolinite, and montmorillonite), quartz, and amorphous silicon (Reid and others, 2003), which rather than contributing to dissolved load in rivers would contribute to the solid phases in soils, as has been observed on carbonate islands such as Bermuda (Herwitz and others, 1996). The dust contribution is also small compared to suspended-solid yields, which range from about 320 to 2,100 t km^{-2} yr^{-1} (table 1).

The slope, C_1, of the regression of the relation of $\log(Si(OH)_4)$ to $\log(R)$ is least negative in the Canóvanas watershed and most negative in the Icacos and Guabá (table 4) watersheds. These slopes are more negative than the slope (C_1) of most rivers studied by Godsey and others (2009), indicating less of a chemostat-like response (more dilution). Regressions on the primary data demonstrate no curvature.

Unusually low $Si(OH)_4$ concentrations were observed in the granitic, forested Icacos watershed (and its subwatershed, the Guabá) on the falling stage of some high-runoff hurricanes and frontal storms (fig. 4 and appendix 1, figs. 4, 5). Some samples (which plot below the constant-input line anchored to average base flow; see fig. 4) had $Si(OH)_4$ yields that were even less than base flow yields, indicating that water that would normally drain from deep in the soil was not doing so during these events. Such low-$Si(OH)_4$ events were not observed, even during the same storms, in the volcaniclastic watersheds (Mameyes and Canóvanas) or in the granitic watershed with an agricultural land-use history (Cayaguás). Soils on the volcaniclastic rocks are more dense, clay-rich, and less permeable (Murphy and Stallard, 2012), whereas the Cayaguás watershed has been deeply eroded and trampled by cattle (Brown and others, 1998; Larsen and Santiago-Román, 2001); it is possible that the mechanism for low-$Si(OH)_4$ waters involves soil porosity. Yield reductions indicate that pathways for deeper groundwater flow in the forested, granitic watersheds were being restricted or even reversed during such storms. It is possible that sediment or litterfall is mobilized in such a way that shallow soil pore spaces in lower slopes and along channels, including macropores, become clogged. This clogging would lead to decreased groundwater seepage and hence lower $Si(OH)_4$ concentrations. Most of the low-$Si(OH)_4$ events occurred prior to the 1998 Hurricane Georges (which was not a low-$Si(OH)_4$ event). Georges was a category 2 hurricane that struck eastern Puerto Rico directly and caused substantial forest damage (Lugo and Frangi, 2003). This damage may have led to changes in soil properties and flow paths. It is also possible that earthworms, which are quite active in these forests (Larsen and others, 2012) and increase soil porosity, may have had their activity reduced by Georges. Finally, it is possible that low-$Si(OH)_4$ events may have occurred, but were not sampled, following Georges. Regardless of the reason, because of their occasional and enigmatic nature, the low-$Si(OH)_4$ events were excluded from the LOADEST calculations.

Chloride

Chloride is derived almost exclusively from seasalt entrained in the atmosphere, and it is primarily deposited as rain (rather than as dry deposition) in the Luquillo Mountains (Heartsill-Scalley and others, 2007; Stallard, 2012a). As with $Si(OH)_4$, Cl^- concentrations typically decrease with increasing runoff in all eastern Puerto Rico WEBB rivers (fig. 5), because a greater proportion of stream water is derived from shallow and overland flow paths, rather than from base flow, during large storms. Base flow contains higher Cl^- concentrations than average rainwater (Stallard, 2012a) because evaporation and transpiration concentrate Cl^- in waters moving downward through the canopy, surface soil, and rooting zone. During high-runoff events, water passing quickly overland and through shallow soils is subjected to proportionately less evaporation and transpiration than during small events (fig. 2). Average Cl^- concentrations are typically greatest in the developed Canóvanas and Cayaguás watersheds (fig. 5). These watershed are drier and have a greater ratio of evapotranspiration to runoff (Murphy and Stallard, 2012), which may concentrate the seasalt contribution.

Because Cl^- does not have a bedrock source, the negative slopes (C_1) of the regression of log (Cl^-) and log(R) (table 4) must reflect dilution of the aged, evaporated water by active storms. The range of slopes is quite narrow, −0.20 to −0.14, presumably reflecting a similar style of mixing among all the watersheds.

Exceptionally high Cl^- concentrations, as much as an order of magnitude greater than average, were recorded in the Mameyes, Icacos, and Guabá watersheds at high runoff rates, primarily during some hurricanes and also during some frontal storms (fig. 5). During Hurricane Georges, a quantity of Cl^- roughly equivalent to 0.3 millimeters (mm) of seawater was deposited over the entire Mameyes watershed (Stallard, 2012a). The Cayaguás watershed, which is leeward of the

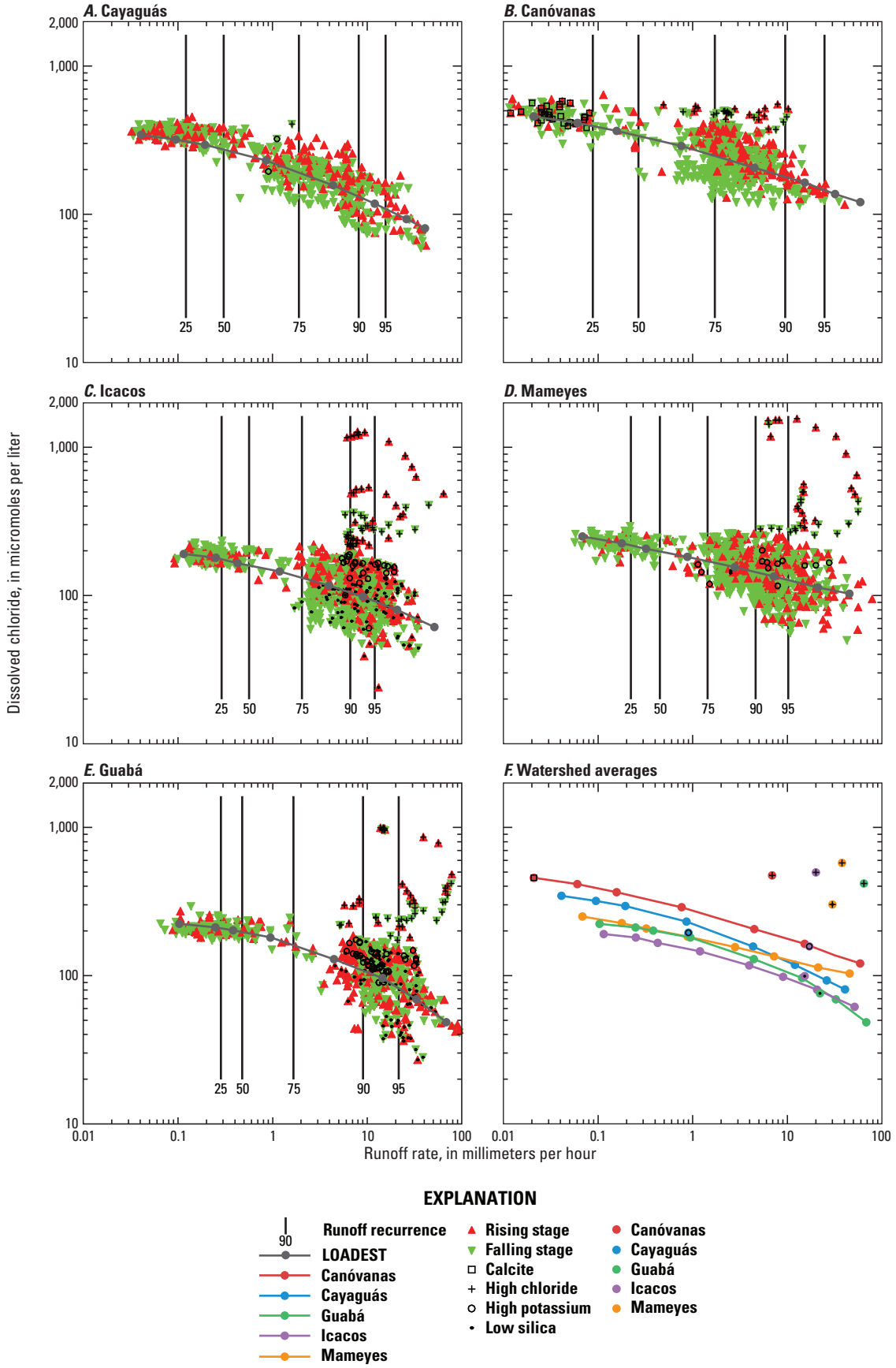
A. Cayaguás
B. Canóvanas
C. Icacos
D. Mameyes
E. Guabá
F. Watershed averages
Dissolved chloride, in micromoles per liter
Runoff rate, in millimeters per hour
2,000
1,000
100
10
0.01
0.1
1
10
100
25
50
75
90
95
EXPLANATION
Runoff recurrence
LOADEST
Canóvanas
Cayaguás
Guabá
Icacos
Mameyes
Rising stage
Falling stage
Calcite
High chloride
High potassium
Low silica
Canóvanas
Cayaguás
Guabá
Icacos
Mameyes

Figure 5 (facing page). Runoff rate–concentration graphs for chloride. Additional sample characteristics are indicated with black symbols: calcite, samples supersaturated with respect to calcite; high chloride, samples with exceptionally high chloride concentrations collected during huge storms; high potassium, samples with high potassium but not high chloride; low silica, Icacos and Guabá samples with unusually low silica concentrations for the runoff rate. The points separated from the watershed-average curves (F) represent the averages of the classes of sample indicated by the superimposed character. These samples are not included in LOADEST models.

Luquillo Mountains and is the farthest inland of the Puerto Rico WEBB watersheds, did not demonstrate any high-Cl^- events; the Canóvanas, on the western flank of the mountains, demonstrated subdued events. This pattern suggests that most of the high-Cl^- rainwater is deposited on the windward side of the Luquillo Mountains. Substantial atmospheric loadings of Cl^- (along with Na^+, NO_3^- and SO_4^{2-}) to the Icacos watershed were also noted by Peters and others (2006). Presumably, the high concentrations are related to high winds and breaking waves in the ocean upwind of the watersheds (Stallard, 2012a). Because the high-Cl^- events have no relation to the explanatory variables (discharge, time, and seasonality) used in LOADEST, they were excluded from the LOADEST regressions. Our estimates of yields of Cl^- and all constituents associated with seasalt are therefore slightly lower than if high-Cl^- samples were included. We do not know how much lower, because the National Atmospheric Deposition Program dataset (which was used to estimate Cl^- inputs) has major data gaps, many during storms (including Hurricane Georges); however, the overall error appears to be small (Stallard, 2012a).

Calcium, Magnesium, and Sodium

Dissolved Ca^{2+}, Mg^{2+} and Na^+ are dominated by a bedrock weathering source, but they can have appreciable atmospheric inputs from seasalt (Mg^{2+} and Na^+) or minor soluble desert dust (Ca^{2+}) (Stallard, 2012a). The concentrations of Ca^{2+}, Mg^{2+}, and Na^+ in all of the study watersheds usually decreased with increasing runoff (fig. 6, table 3), and falling stages tended to have lower concentrations than rising stages. Stream samples from the Mameyes and Canóvanas watersheds contained distinctly elevated Ca^{2+} concentrations compared with the other study watersheds, and the Canóvanas also contains contained elevated Mg^{2+} (fig. 6). The bedrock of these volcaniclastic watersheds is somewhat richer in Ca^{2+}-bearing and Mg^{2+}-bearing silicate minerals than the granitic watersheds (Jolly and others, 1998; Smith and others, 1998; Stallard, 2012b). Minor bedrock carbonate minerals, which can be a source of abundant Ca^{2+} and sometimes Mg^{2+} (Stallard, 1995a,b), have been documented in the bedrock units underlying the Canóvanas and Mameyes watersheds (Murphy and others, 2012). Rivers draining carbonate-rich watersheds in western Puerto Rico demonstrated only minor drops in conductivity through major storm events (Haire, 1972) because carbonate rocks dissolve rapidly. All eastern Puerto Rico WEBB watersheds, in contrast, showed decreases in conductivity with increasing runoff (fig. 3), suggesting that the elevated Ca^{2+} and Mg^{2+} were not caused by the carbonate minerals but rather by the silicate minerals.

Sodium concentrations, similar to concentrations of Cl^-, were typically highest in the developed Canóvanas and Cayaguás watersheds. This pattern may be due to a greater ratio of evapotranspiration to runoff in these drier watersheds (Murphy and Stallard, 2012), which would concentrate the seasalt contribution, or due to domestic inputs (or both). Low-$Si(OH)_4$ samples tended to also have slightly lower Ca^{2+} (fig. 6), although the effect was not pronounced, indicating that the mechanism causing low $Si(OH)_4$ may affect other bedrock-derived constituents.

All three cations demonstrate high concentrations during the high-runoff, high-Cl^- events discussed earlier in the Chloride section. Accordingly, the cation concentration data for these samples were excluded from the LOADEST calculations and regressions.

For all study watersheds, comparison of the slopes (C_1) of Ca^{2+}, Mg^{2+}, Na^+, and Cl^- for the regression of log(C) and log(R) demonstrates that the slope of Ca^{2+} is the most negative, followed by Mg^{2+}, then Na^+, and finally Cl^- (table 4). This order represents a continuous variation from constituents derived primarily from bedrock weathering to those derived from seasalt, and it is consistent with a mix of the two sources: bedrock weathering deep in the profile, and evaporated rainfall, distributed more widely through the soil profile.

Dissolved Organic Carbon

Dissolved organic carbon is uniquely derived from plant material, either as the product of breakdown or as exudates (Stumm and Morgan, 1981). The ultimate source of DOC is atmospheric carbon dioxide fixed through photosynthesis. DOC was slightly greater in the developed watersheds, perhaps reflecting the differences in land cover or the effects of agricultural on soils. For all watersheds, DOC concentrations increased with increasing runoff rates and reached a rough peak in the 75 to 90 percent or 90 to 95 percent runoff percentiles (table 3). At the very highest runoff rates, DOC concentrations tended to decrease, and differences among the watersheds lessened (fig. 7). This trend was also observed by Shanley and others (2011), who used other sources to extend the present dataset for the Icacos watershed from 1981 to 2008.

The decrease in concentrations at high runoff could imply a supply limitation, whereby the processes that generate and release DOC cannot supply it at a rate that compensates for the increased throughput of water. However, DOC concentrations are highest on falling stages (fig. 7), opposite to what is expected from a supply limitation.

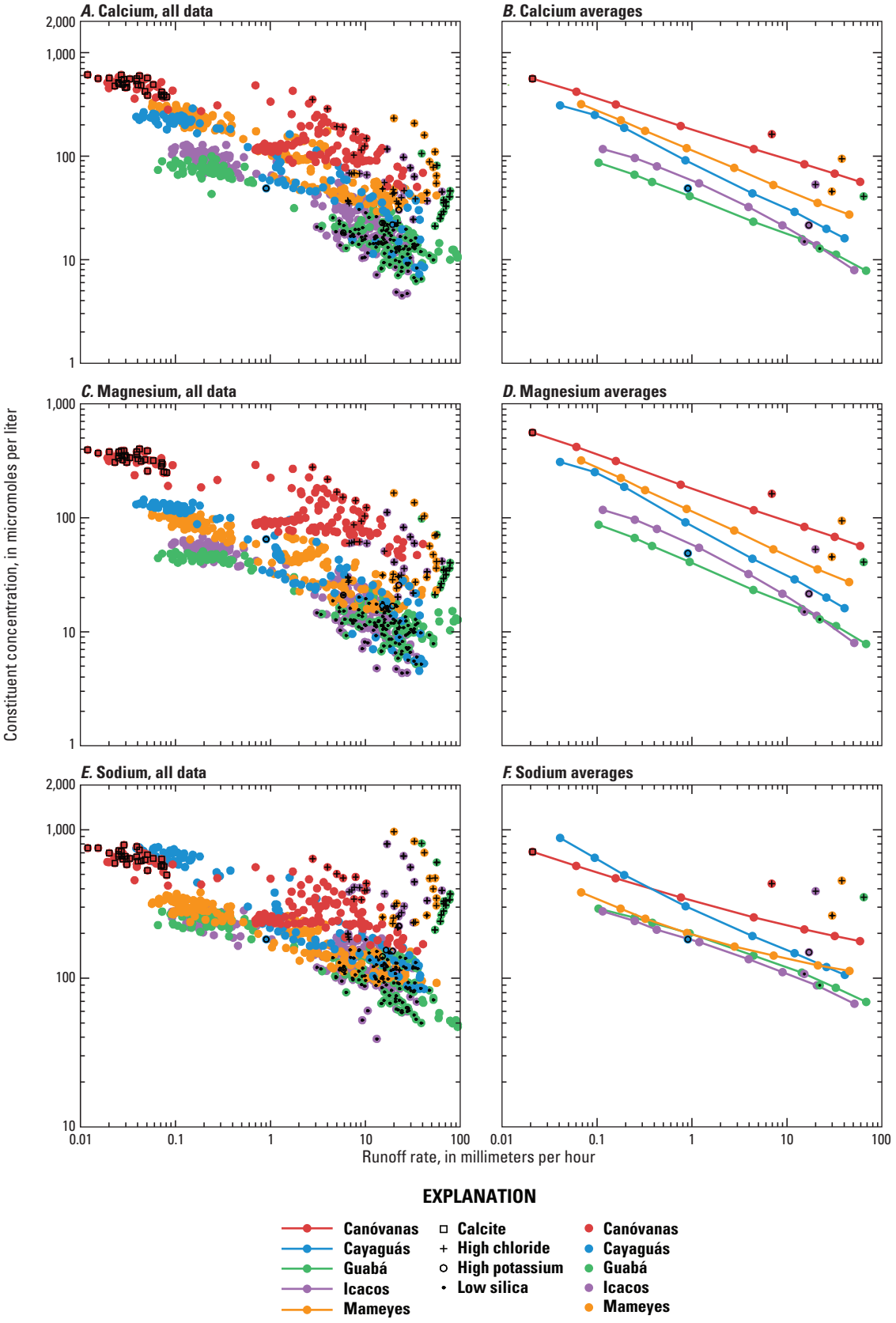
A. Calcium, all data
B. Calcium averages
C. Magnesium, all data
D. Magnesium averages
E. Sodium, all data
F. Sodium averages
Constituent concentration, in micromoles per liter
Runoff rate, in millimeters per hour
2,000
1,000
100
10
1
0.01
0.1
1
10
100
EXPLANATION
Canóvanas
Cayaguás
Guabá
Icacos
Mameyes
Calcite
High chloride
High potassium
Low silica

Figure 6 (facing page). Runoff rate–concentration graphs for calcium, magnesium, and sodium ions. The left diagrams represent the Water, Energy, and Biogeochemical Budget program dataset. The right diagrams represent averages calculated from hourly estimates determined using LOADEST. Additional sample characteristics are indicated with black symbols; calcite, samples supersaturated with respect to calcite; high chloride, samples with exceptionally high chloride concentrations collected during huge storms; high potassium, samples with high potassium but not high chloride; low silica, Icacos and Guabá samples with unusually low silica concentrations for the runoff rate. The points separated from the watershed-average curves (B, D, F) represent the averages of the classes of sample indicated by the superimposed character. These samples are not included in LOADEST models.

Alternatively, a DOC decrease with increasing runoff rate may reflect a change to flow paths that involves less interaction and contact time with soil organic matter. At lowest runoff rates, stream water has moved through deep soils, deeper riparian zones, and hyporheic zones (fig. 2). With the exception of the hyporheic zone, these zones contain relatively little organic matter. At intermediate runoff rates, more water is presumably moving through shallow-soil pathways and riparian zones which, if present, are likely to be flooding; this flooding would represent optimum conditions for interacting with shallow-soil organic matter. Finally, at the highest runoff rates, overland flow is important because it reduces the overall interaction of water with organic matter. At runoff rates of roughly 3 to 10 mm h^{-1} DOC concentrations begin their substantial decline, reflected by the downward curvature of diagrams shown in fig. 7. This decline suggests that this range of runoff rates may mark a transition to a regime where overland flow and associated reduced soil interaction become important. Regardless of the mechanism, these data show that the highest discharge classes (greater than 90 percent) must be included when one calculates DOC loads and yields from watersheds. Without the high-runoff data, yields will be overestimated.

The curves of averaged concentrations based on LOADEST calculations do not always pass through the middle of the concentration-data field at middle-range runoff rates (fig. 7). A likely factor is the lower collection density of middle-range runoff samples (appendix 1), which will not alias the regression residual as strongly.

For every study river, the regression of log(DOC) on log(R), using the primary data, has statistically significant downward curvature. The position of the peak is calculated for the zero of the first derivative

$$\text{Peak} = 10^{(-C_1/(2 \cdot C_2))}$$

and peaks range from 2.5 mm h^{-1} to 8.6 mm h^{-1}.

The Nutrients: Nitrate, Ammonium Ion, Phosphate, and Potassium

Nitrate, NH_4^+, $-PO_4^{3-}$ and K^+ are considered to be the principal plant nutrients. Of these, throughfall is especially enriched in NH_4^+, $-PO_4^{3-}$ and K^+ when compared with rainwater (Heartsill-Scalley, 2007). Nitrate and NH_4^+ have atmospheric sources, either dissolved in precipitation or as a result of plant fixation. Both can be lost from a watershed by conversion back to gaseous forms. Phosphate is primarily derived from bedrock, but it can also be deposited in eastern Puerto Rico as Saharan dust (Pett-Ridge and others, 2009b). Phosphate is an important plant nutrient that is also easily sequestered by chemical reactions with Al^{3+} or Fe^{3+} ions; distinguishing these two mechanisms of $-PO_4^{3-}$ removal is difficult. Potassium is mostly bedrock derived but can also be atmospherically deposited in seasalt (some K^+ arrives in Saharan dust, but in the form of insoluble clay minerals; Reid and others, 2003). Potassium and NH_4^+ can be weakly held on cation-exchange sites in soil. In the developed watersheds, all of these nutrients can be added by manmade products such as fertilizers or by domestic or industrial wastes.

The runoff-concentration relations for K^+, NO_3^-, NH_4^+, and $-PO_4^{3-}$ sometimes demonstrate considerable scatter (figs. 8, 9), and diagrams of these relations do not demonstrate the steeply decreasing curves observed for $Si(OH)_4$, Cl^-, Ca^{2+}, Mg^{2+}, and Na^+. For each nutrient at almost every runoff rate, the concentration-runoff curves representing the developed watersheds (Canóvanas and Cayaguás) illustrate substantially higher concentrations than those representing the forested watersheds (figs. 8, 9); it is likely that this difference reflects human inputs, such as fertilizers or agricultural and domestic wastes. Precise identification of sources would require detailed surveys that were not part of this study.

A number of high-runoff samples from the Mameyes, Icacos, and Guabá watersheds demonstrated elevated K^+ concentrations (fig. 8). These samples, however, did not have high concentrations of Cl^-, so elevated K^+ probably was not caused by windblown seasalt. These high-K^+ events were recorded in the Icacos and Guabá watersheds only during the year after Hurricane Georges (1998–1999) and in the Mameyes watershed mostly after Georges (appendix 1, figs. 1–5). After Hurricane Hugo in 1989, stream-water concentrations of K^+, NO_3^-, and NH_4^+ doubled and remained elevated for almost 2 years; K^+ and NO_3^- returned to average concentrations at the same time that the canopy recovered, suggesting biological control on the cycling of these ions (Schaefer and others, 2000; concentrations of Na^+, Mg^{2+}, Ca^{2+}, Cl^-, and SO_4^{2-} showed little effect). The elevated K^+ concentrations are consistent with other post-Hurricane Georges observations that indicate the release of K^+ from litter (Ostertag and others, 2003). The high-K^+ events in this study, however, did not appear to be associated with higher concentrations of either $-PO_4^{3-}$ or NH_4^+; also, not all the storms in the year following the hurricane resulted in high K^+ concentrations. It is possible that the absence of high concentrations of either $-PO_4^{3-}$ or NH_4^+ was a sampling

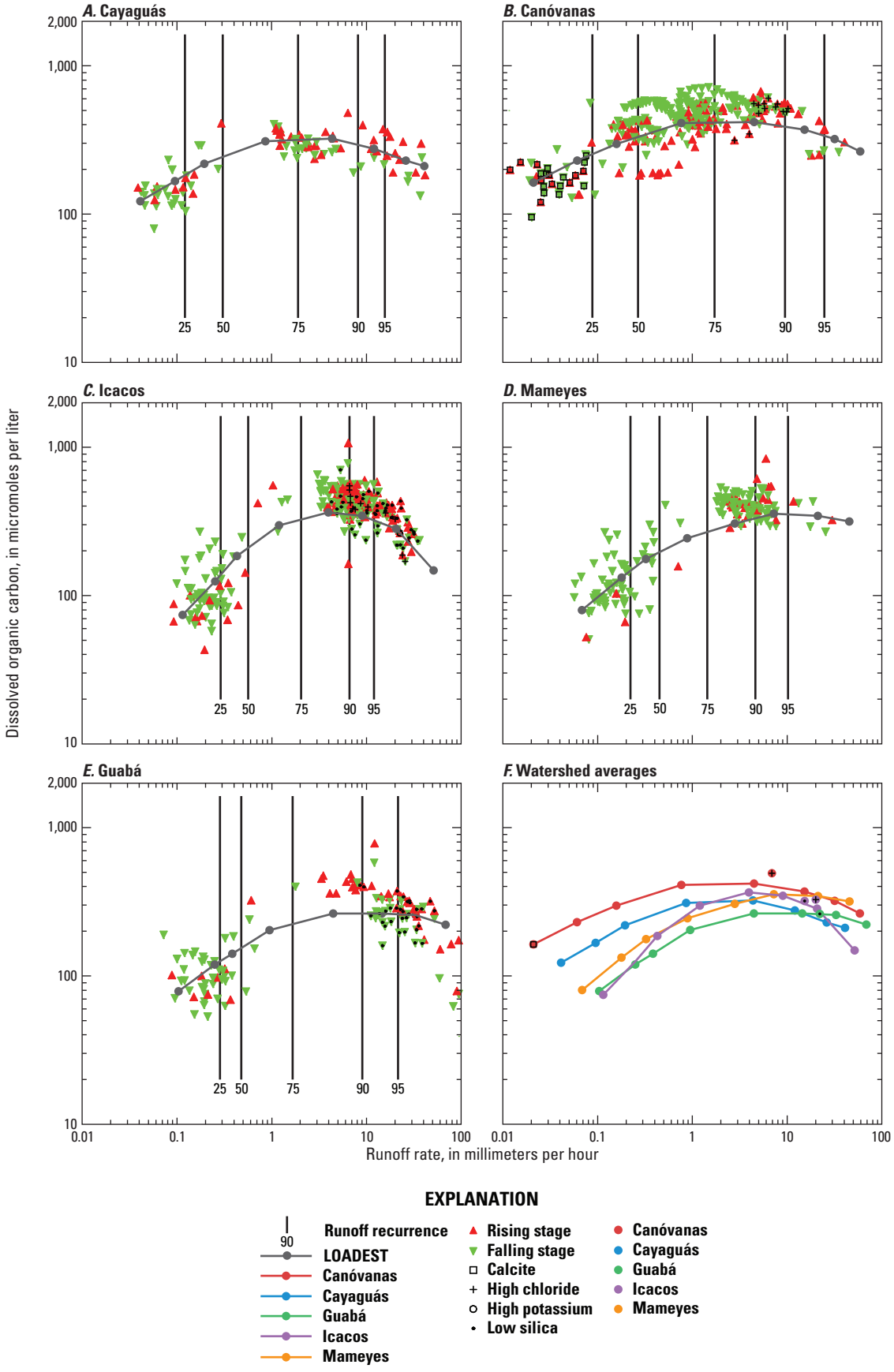
A. Cayaguás
B. Canóvanas
C. Icacos
D. Mameyes
E. Guabá
F. Watershed averages
Dissolved organic carbon, in micromoles per liter
Runoff rate, in millimeters per hour
2,000
1,000
100
10
0.01
0.1
1
10
100
25
50
75
90
95
EXPLANATION
Runoff recurrence
LOADEST
Canóvanas
Cayaguás
Guabá
Icacos
Mameyes
Rising stage
Falling stage
Calcite
High chloride
High potassium
Low silica

Figure 7 (facing page). Runoff rate–concentration graphs for dissolved organic carbon. Additional sample characteristics are indicated with black symbols: calcite, samples supersaturated with respect to calcite; high chloride, samples with exceptionally high chloride concentrations collected during huge storms; high potassium, samples with high potassium but not high chloride; low silica, Icacos and Guabá samples with unusually low silica concentrations for the runoff rate. The points separated from the watershed-average (F) curves represent the averages of the classes of sample indicated by the superimposed character.

artifact, because K^+ was analyzed in considerably more samples than $-PO_4^{3-}$ or NH_4^+, and analytical errors for K^+ are relatively smaller (appendix 2).

Some samples from the Icacos, Guabá, and Mameyes watersheds demonstrated especially low NO_3^- concentrations (fig. 9). These samples, which were collected during hurricanes, also always have high Cl^- concentrations. Hurricanes derive their energy and moisture from maritime air masses that presumably lack a strong contribution of pollutants, such as NO_3^-, from continents.

Regardless of the reason, because of their occasional and enigmatic nature, the high-K^+ samples and low-NO_3^- samples collected during high-Cl^- events have no obvious relation to the explanatory variables used in LOADEST, so these solutes for these samples were excluded from the LOADEST calculations.

Sulfate

Sulfur derives from a complex array of geologic and atmospheric sources. Geologic sources include reduced sulfur from sulfides, pyrite, and (rarely) elemental sulfur, and from sulfate salts from minerals such as anhydrite and gypsum. Minor sulfides and pyrite are found in small mineralized zones surrounding the Río Blanco intrusion in the Luquillo Mountains (Murphy and others, 2012). Atmospheric sources of sulfur include seasalt, Saharan dust (in the form of anhydrite and gypsum; Reid and others, 2003), volcanic eruptions, burning of fossil fuels, and reduced sulfur gases from marine and terrestrial sources (Stallard and Edmond, 1981; Andreae and Andreae, 1988; Stallard, 2012a). Atmospheric sulfur is deposited as SO_4^{2-}. Sulfur, like organic carbon, NO_3^-, and NH_4^+, can be lost from a watershed as a gas (Stallard, 2012a).

The runoff-concentration relations for SO_4^{2-} in the Puerto Rico WEBB watersheds differed substantially (fig. 10). Sulfate concentrations were generally lowest in the forested, granitic watersheds (Icacos and Guabá) and highest in the developed watersheds (Canóvanas and Cayaguás). Sulfur concentrations in the forested, volcaniclastic Mameyes watershed were similar to those in the developed watersheds at low runoff rates, but at high runoff rates, concentrations were similar to those in the Icacos and Guabá watersheds (fig. 10). The Icacos and Guabá watersheds have runoff-concentration curves that are relatively flat (similar to the curves of DOC and nutrients), whereas SO_4^{2-} concentrations in the remaining watersheds decrease with increasing runoff (similar to the constituents that are not particularly bioactive and have substantial bedrock and atmospheric sources: Na^+, Mg^{2+}, and Ca^{2+}). Owing to the low level of human activity in the Mameyes watershed, the high concentrations at low runoff probably reflected a geologic source. It is hard to say whether the high concentrations at low discharge in the Canóvanas and Cayaguás are entirely natural or are influenced by minor contamination, because without detailed investigation, it would be difficult to distinguish an exclusively geologic source from one with added human inputs, such as fertilizers.

Sulfate-to-Cl^- ratios provide information about sources of sulfur (Stallard and Edmond, 1981). The SO_4^{2-}-to-Cl^- mole ratio of seasalt, 0.051, is the lowest of all SO_4^{2-} sources; precipitation in eastern Puerto Rico has a higher average SO_4^{2-}-to- Cl^- ratio (about 0.106), because it contains not only seasalt but also sulfur from gas phase and dust sources (Stallard, 2012a). Sulfate-to-Cl^- ratios in stream samples from the developed, farther-inland watersheds (Canóvanas and Cayaguás) are always greater than the rainfall ratio and increase with runoff, perhaps reflecting an increased contribution of SO_4^{2-} from vegetation or agricultural fertilizers (fig. 10). The forested, volcaniclastic Mameyes watershed also has SO_4^{2-}-to-Cl^- ratios greater than the rainfall ratio (except for high Cl^- events), but these ratios decrease slightly with increasing runoff. The SO_4^{2-}-to-Cl^- ratios in samples from the forested, granitic watersheds (Icacos and Guabá) are exceptionally low (equal to or below the seasalt ratio) at low runoff rates, and they increase to ratios above rainwater at high runoff rates (except for high-Cl^- events). The exceptionally low ratios at low runoff may be due to the transformation of SO_4^{2-} into reduced sulfur gases (such as dimethyl sulfide) in the soil, whereupon the sulfur is emitted to the atmosphere (Stallard and Edmond, 1981). Alternatively, these watersheds may have no substantial geologic source of sulfur, and because sulfur is a nutrient (a part of some amino acids), it should be retained in biomass and organic matter in shallow soils (such as N, P, and K) during lower-runoff conditions only to be subsequently released to the stream during high-runoff events. Soil chemical analyses (Stallard, 2012b), however, show no sulfur in mineral soil or stream sediment.

Alkalinity, Carbon Dioxide, and Calcite Saturation

Alkalinity is the amount of anion charge per unit volume that can be titrated with a strong acid to reach the first equilibrium endpoint for the CO_2 system (Stumm and Morgan, 1981). Alkalinity is a conservative property. The primary source of alkalinity is the weathering of silicate and carbonate minerals; it can be modified by addition or loss of NO_3^-, NH_4^+, organic acids, and sulfuric acid from sulfide weathering and acid precipitation. Higher alkalinities tend to be associated with higher pH values, but for a given alkalinity, the vapor pressure of CO_2 controls pH.

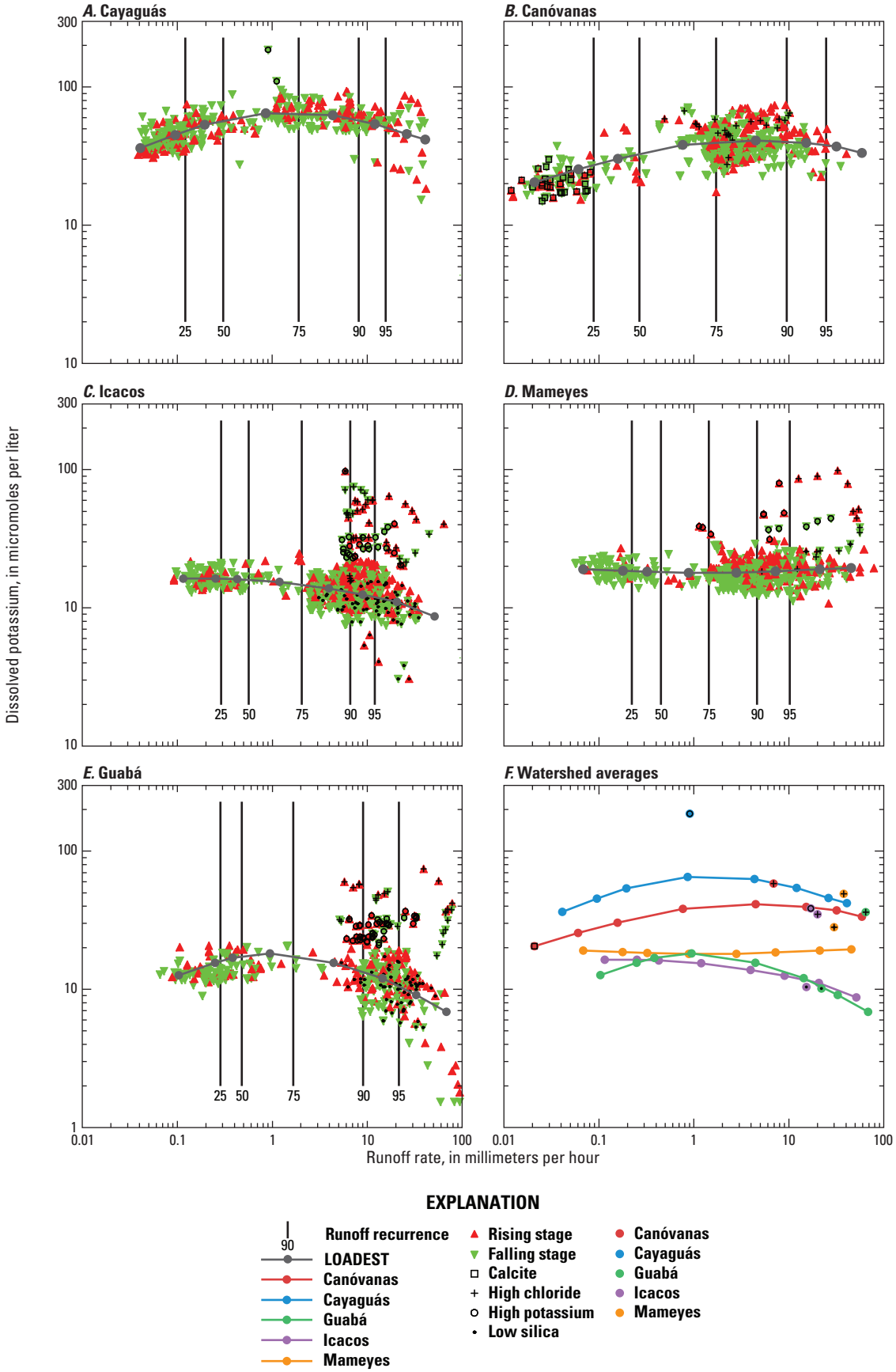
A. Cayaguás
B. Canóvanas
C. Icacos
D. Mameyes
E. Guabá
F. Watershed averages
Dissolved potassium, in micromoles per liter
Runoff rate, in millimeters per hour
300
100
10
1
0.01
0.1
1
10
100
25
50
75
90
95
EXPLANATION
Runoff recurrence
LOADEST
Canóvanas
Cayaguás
Guabá
Icacos
Mameyes
Rising stage
Falling stage
Calcite
High chloride
High potassium
Low silica
Canóvanas
Cayaguás
Guabá
Icacos
Mameyes

Figure 8 (facing page). Runoff rate–concentration graphs for potassium ion. Additional sample characteristics are indicated with black symbols; calcite, samples supersaturated with respect to calcite; high chloride, samples with exceptionally high chloride concentrations collected during huge storms; high potassium, samples with high potassium but not high chloride; low silica, Icacos and Guabá samples with unusually low silica concentrations for the runoff rate. The points separated from the watershed-average curves (F) represent the averages of the classes of sample indicated by the superimposed character. These samples are not included in LOADEST models.

The study-area rivers draining volcaniclastic rocks tend to have higher alkalinities than rivers draining granitic rocks (fig. 11). Two geologic factors may contribute to this situation: the volcanic rocks have higher concentrations of Ca^{2+} and Mg^{2+} compared with the granitic rocks (Jolly and others, 1998; Smith and others, 1998), and minor calcite is present in some of the volcaniclastic rocks (Murphy and others, 2012). Negative alkalinity (that is, acidity) is observed in event samples collected at the highest runoff rates in the Icacos and Guabá watersheds, reflecting the importance of the various acid inputs, such as acid rain, nitrate formation, and DOC, to these watersheds.

The partial pressure of carbon dioxide (P_{CO_2}), CO_2 saturation, and the saturation index for calcite, $SI_{calcite}$, were calculated from alkalinity, temperature, and pH following Stumm and Morgan (1981; appendix 1). These parameters are useful in assessing the state of carbonate-system thermodynamics and, when combined with O_2, they can be used to identify in-stream respiration. Oxygen is a bioactive gas that is readily exchanged between water and the atmosphere and is linked to CO_2 through photosynthesis, respiration, decay, and combustion. Using CH_2O as chemical shorthand for organic matter, the photosynthesis reaction is simple:

$$\underset{\text{photosynthesis}\rightarrow}{\overset{\leftarrow\text{decay, respiration}}{CO_2 + H_2O \leftrightarrow CH_2O + O_2.}}$$

According to this biologically mediated reaction, when the concentration (and hence degree of saturation) of CO_2 rises, O_2 should fall (the reverse is true for combustion, decay, and respiration). The degree of saturation of both gases should rise with an increase in temperature.

The rivers that drain granitic bedrock (Icacos, Guabá, and Cayaguás) have higher degrees of CO_2 saturation, whereas the rivers that drain volcaniclastic bedrock (Mameyes and Canóvanas) are only slightly oversaturated or are even undersaturated (fig. 11). The rivers that drain granitic rocks are less steep and turbulent than those that drain volcaniclastic rocks, and therefore they probably have greater exchange with flood plains and sandy beds. Turbulent flow and rapid gas exchange as rivers cascade over steep rocky beds in the volcaniclastic watersheds would drive the water towards equilibrium with the atmosphere. The few grab samples collected from the Icacos watershed at high runoff rates are close to saturation, indicating that this river equilibrates with the atmosphere when the river is quite turbulent. The undersaturation of CO_2 (fig. 11), primarily in the Canóvanas watershed, is probably due to in-channel photosynthesis by aquatic plants, which raises pH and O_2 (fig. 3) and reduces CO_2. In all the other rivers, CO_2 is usually supersaturated and O_2 undersaturated, indicating a dominance of respiration and decay.

The undersaturation of CO_2 caused by in-stream photosynthesis appears to have driven the high-alkalinity Canóvanas water into supersaturation with respect to calcite at low-runoff conditions (fig. 11). Evidence of calcite precipitation, such as tufa deposits, has not been investigated. The lack of abundant limestone or calcite-bearing bedrock in the Canóvanas watershed suggests that the source of the supersaturated waters is silicate weathering, perhaps accompanied by minor calcite weathering. Soil solutions equilibrate with the high-CO_2 environment of soils and outgas once groundwater enters the channel. The outgassing could lead to calcite supersaturation.

Suspended Sediment

Three sources contribute suspended sediment to the eastern Puerto Rico WEBB watersheds: surficial erosion, landslides, and bed and bank erosion (Larsen, 2012). This sediment can either be transported out of the watershed by rivers or stored in the watershed as colluvium and alluvium. Suspended sediment concentrations in all rivers are low except during major storms when they increase rapidly with runoff rate (fig. 12). All of the LOADEST curves have a slight downward curvature, except for the Icacos watershed. For the Canóvanas and Cayaguás watersheds, runoff must exceed the 50th percentile of runoff rate before concentrations of 100 milligrams per liter are reached; for the Icacos and Guabá, the 75th percentile must be exceeded, and for the Mameyes, the 90th percentile must be exceeded (table 4). A few samples from highest runoff rates in the Cayaguás, Canóvanas, and the Icacos watersheds had exceptionally high concentrations of suspended sediment; one Icacos sample contained more than 100 grams per liter. The cause of these high concentrations is unknown. The Icacos and Cayaguás river beds are very sandy; in fact, sand is extracted commercially in the Río Cayaguás. It is possible that the bed was substantially mobilized and that the water intake nozzle of the sampler, which is not far above the river bed, may have been in the boundary layer. Alternatively, several major events have caused landslides to fall directly into the Icacos channel, so these high concentrations may reflect diluted debris flows.

The suspended-sediment yields reported here are considerably greater than yields reported in all previous estimates (McDowell and Asbury, 1994; Brown and others, 1995; Larsen, 1997; Larsen and Stallard, 2000). The yields reported here reflect the large events captured during the Puerto Rico WEBB program, and they allow the relation between

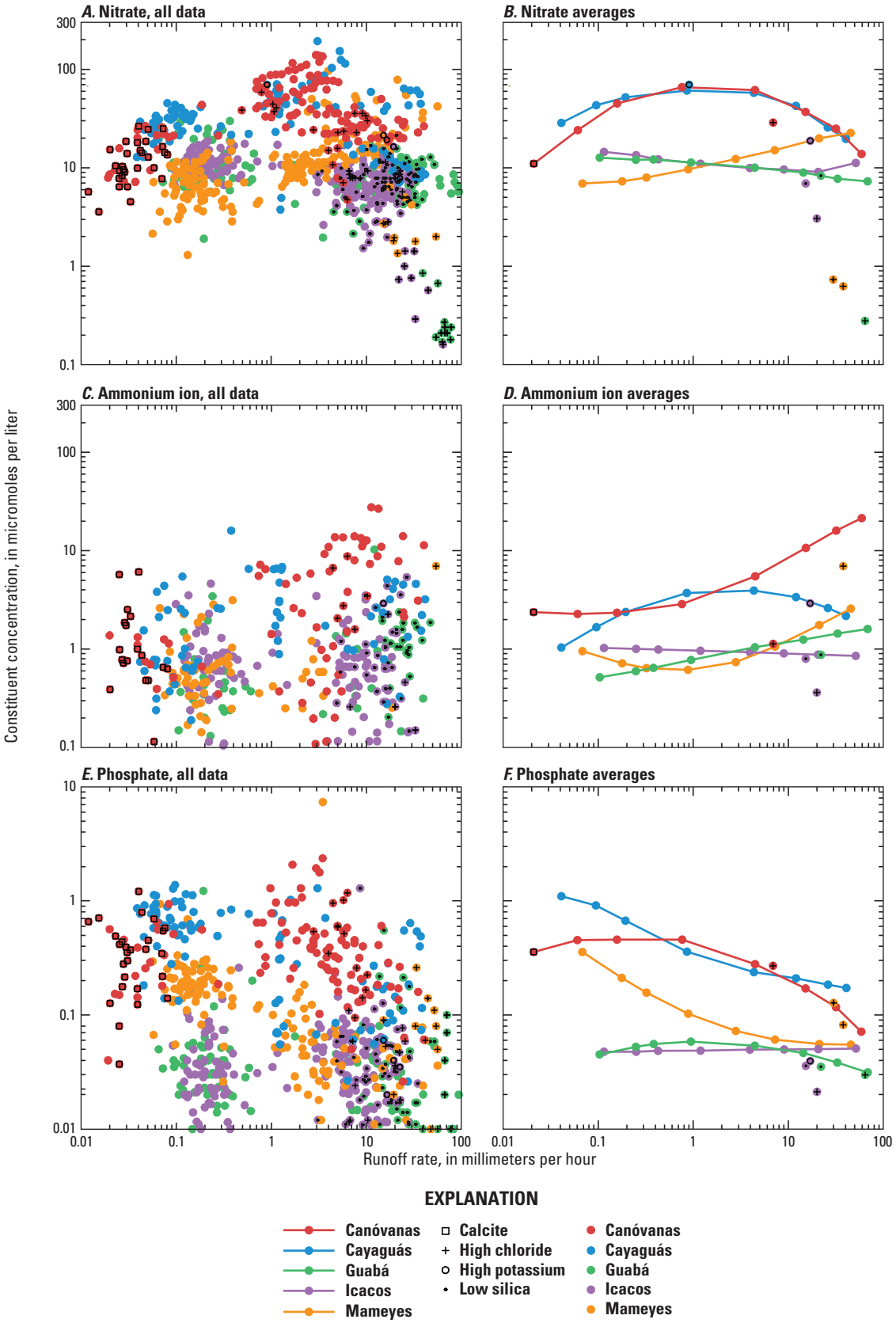
A. Nitrate, all data
B. Nitrate averages
C. Ammonium ion, all data
D. Ammonium ion averages
E. Phosphate, all data
F. Phosphate averages
Constituent concentration, in micromoles per liter
Runoff rate, in millimeters per hour
EXPLANATION
Canóvanas
Cayaguás
Guabá
Icacos
Mameyes
Calcite
High chloride
High potassium
Low silica
Canóvanas
Cayaguás
Guabá
Icacos
Mameyes

Figure 9 (facing page). Runoff rate–concentration graphs for nitrate, ammonium ion, and phosphate ions. Additional sample characteristics are indicated with black symbols; calcite, samples supersaturated with respect to calcite; high chloride, samples with exceptionally high chloride concentrations collected during huge storms; high potassium, samples with high potassium but not high chloride; low silica, Icacos and Guabá samples with unusually low silica concentrations for the runoff rate. The points separated from the watershed-average curves (B, D, F) represent the averages of the classes of sample indicated by the superimposed character. These samples are not included in LOADEST models.

suspended sediment and runoff rate to be characterized at much higher runoff rates than ever before. In addition, the period 1996 to 2005 was a much wetter period than during previous studies.

Sediment yields from all watersheds were considerably greater than Saharan dust loadings of about 21±7 t km^{-2} yr^{-1} (Pett-Ridge and others, 2009b). This relation indicates that Saharan dust is probably not a major component of the mass budget in this landscape.

Conclusions

The water quality of the eastern Puerto Rico WEBB rivers, in terms of pH, dissolved oxygen, dissolved constituents, and suspended solids, is quite good, despite evidence of amphibian die-offs and increasing atmospheric deposition of nitrate. Despite substantial differences in land cover, annual runoff, or bedrock type, the water quality of these WEBB rivers is not marked by extreme contrasts. The yields of constituents derived largely from bedrock weathering (Ca^{2+}, alkalinity, and $Si(OH)_4$), from seasalt (Cl^-), or from a mix of the two sources (Na^+, Mg^{2+}, K^+, and SO_4^{2-}) differed by a factor of less than 2 among all watersheds, showing little relation to land cover, annual runoff, or bedrock type. Average concentrations of these constituents tended to be higher in the developed, leeward watersheds (Cayaguás and Canóvanas) compared with the forested, windward watersheds (Icacos, Guabá, and Mameyes). The developed watersheds had substantially higher yields of nutrients (NO_3^-, NH_4^+, and $-PO_4^{3-}$) than the forested watersheds. In-stream productivity in the Canóvanas watershed is sufficiently great to cause oxygen supersaturation. It is possible that concentrations of some constituents are higher in the rivers draining the developed, leeward watersheds because of lower mean-annual runoff and higher ratios of evapotranspiration to runoff than is true in the forested, windward watersheds. However, the developed watersheds have higher concentrations of Na^+, Cl^-, SO_4^{2-}, K^+, NO_3^-, NH_4^+, and $-PO_4^{3-}$ at a given discharge; this constituent profile, along with the higher nutrients yields, suggests that additional sources, most likely human activities related to agriculture and domestic waste rather than to evapotranspiration, are causing the difference. Suspended-sediment yields were generally low during major storms, when a substantial amount of annual sediment export occurred. Suspended sediment yields from the granitic watersheds were about six times as great as from the volcaniclastic watersheds, independent of land cover and mean-annual runoff. The granitic watersheds generated about 2,000 t km^{-2} yr^{-1}; this value is greater than previous estimates of sediment yield from these watersheds and may be due to a wetter sampling period or to the sampling of greater runoff events (or both).

Several anomalous types of water-quality samples were identified. Samples with very high Cl^- concentrations were associated with some hurricanes and other large storms. These samples were associated with elevated concentrations of other ions that are abundant in seasalt (Na^+, K^+, Mg^{2+}, Ca^{2+}, SO_4^{2-}), and often anomalously low NO_3^- concentrations. This composition reflects windborne seasalt from the ocean and a dominance of maritime, rather than continental, air masses contributing to the storms. Hurricane Georges, the largest storm of our study period, led to short-term and long-term changes in water quality in the forested, windward watersheds. The storm itself, like those described above, produced anomalously high concentrations of seasalt-related constituents and low NO_3^- concentrations. For about 1 to 2 years after the hurricane, occasional high-K^+ event samples were recovered that lacked correspondingly high concentrations of Cl^- and other seasalt-related ions; therefore the K^+ cannot be attributed to seasalt inputs. These samples may indicate the release of potassium from litter deposited by the storm, consistent with post-Hurricane Georges observations (Ostertag and others, 2003). Prior to Hurricane Georges, but not after, samples with anomalously low concentrations of silica were recorded in the forested watersheds. The low-silica events may have been caused by a change in hydrologic pathway during some storms that resulted in shallow flow paths; Georges may have led to the clogging or collapse of such macropores and pipes. These anomalous samples were not included in load and yield regressions.

For most constituents, the rivers show similar trends in runoff–dissolved constituent concentration graphs, suggesting considerable similarity in runoff generation and flow path structuring despite differences in geology, soils, and land cover. The nonbioactive, bedrock-derived and atmospherically derived constituents ($Si(OH)_4$, Ca^{2+}, Mg^{2+}, Na^+, and Cl^-) decrease in concentration with increasing discharge. The trends of the primary data are linear, while some curvature is seen for smoothed data. No trends are sigmoidal. These observations are consistent with the permeability-porosity-aperture model. All the slopes, C_1, for all the bedrock- and seasalt-derived constituents tend to be lower than for most of the rivers in the Hydrologic Benchmark Network dataset (which are mostly in the −0.15 to −0.05 range). For a given river, the various slopes of bedrock-derived constituents are not statistically identical. The slope of $Si(OH)_4$, which is exclusively derived from bedrock weathering, differs considerably from that of the

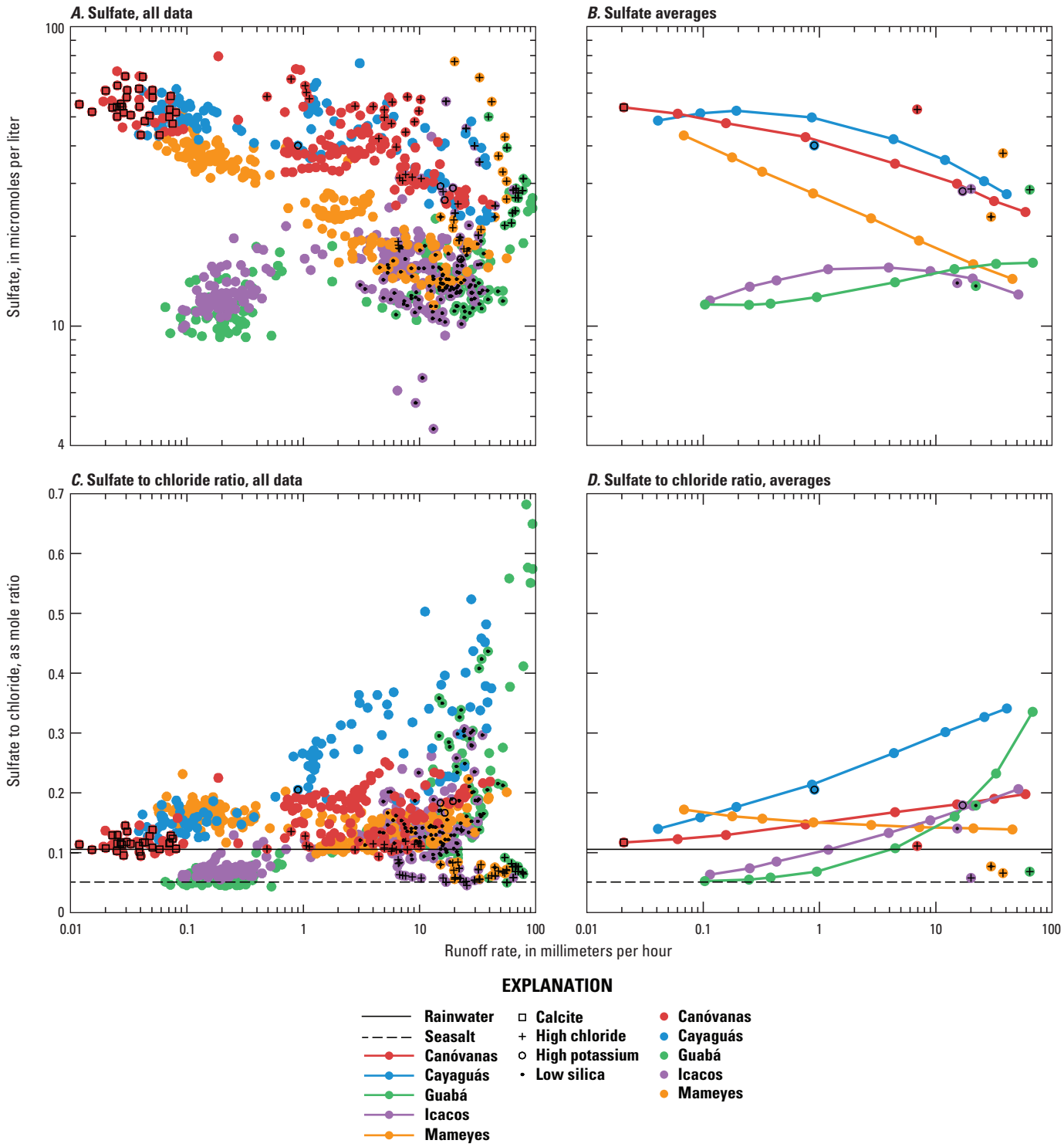

Figure 10. Runoff rate–concentration graphs for sulfate and sulfate:chloride ratio. Additional sample characteristics are indicated with black symbols; calcite, samples supersaturated with respect to calcite; high chloride, samples with exceptionally high chloride concentrations collected during huge storms; high potassium, samples with high potassium but not high chloride; low silica, Icacos and Guabá samples with unusually low silica concentrations for the runoff rate. The points separated from the watershed-average curves (B, D) represent the averages of the classes of sample indicated by the superimposed character. These samples are not included in LOADEST models.

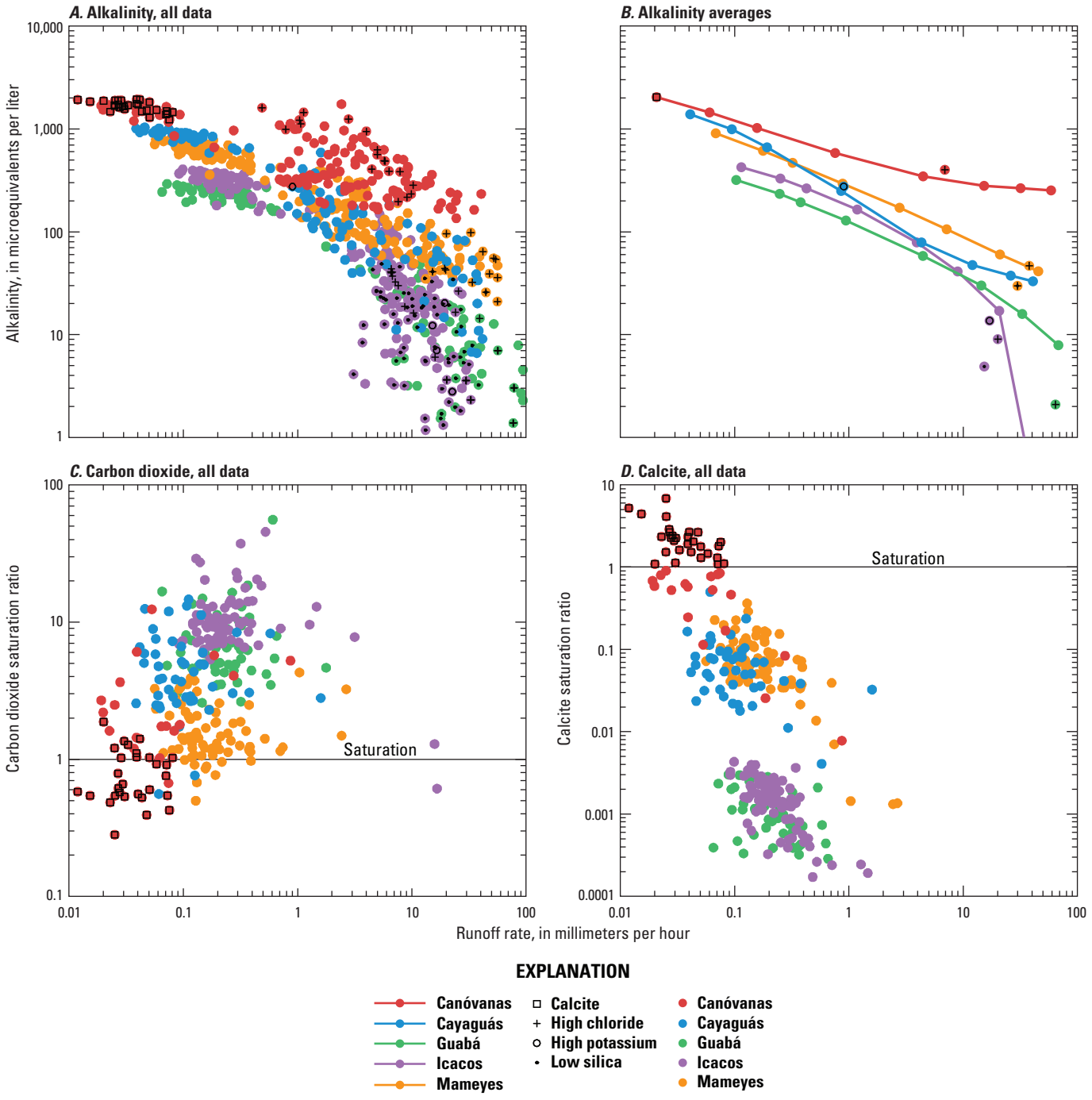

Figure 11. Alkalinity, carbon dioxide saturation, and calcite saturation in the eastern Puerto Rico WEBB rivers, 1991–2005. Additional sample characteristics are indicated with black symbols; calcite, samples supersaturated with respect to calcite; high chloride, samples with exceptionally high chloride concentrations collected during huge storms; high potassium, samples with high potassium but not high chloride; low silica, Icacos and Guabá samples with unusually low silica concentrations for the runoff rate. The points separated from the sample-average curves (B) represent the averages of the classes of sample indicated by the superimposed character. These samples are not included in LOADEST models.

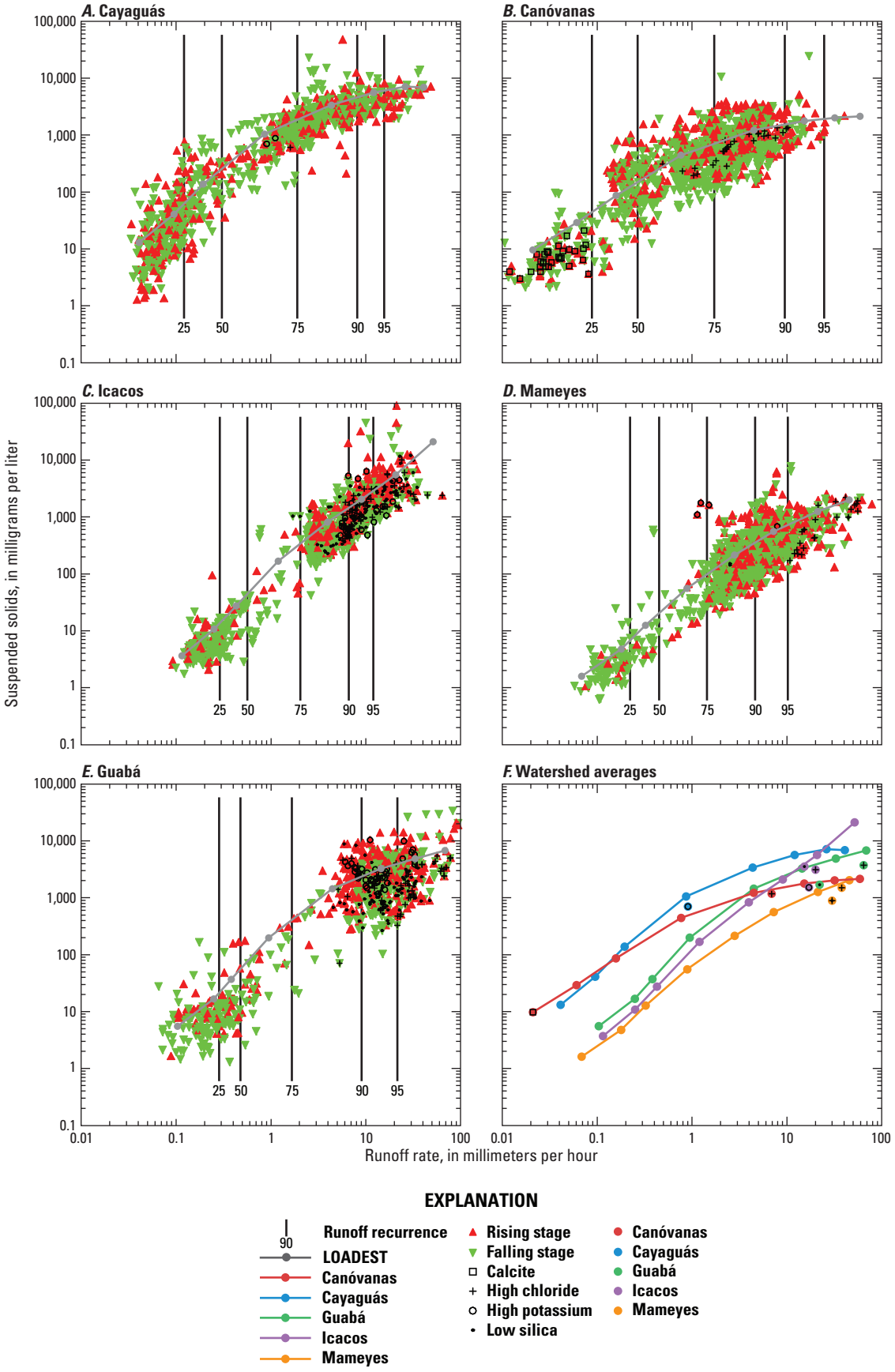
A. Cayaguás
B. Canóvanas
C. Icacos
D. Mameyes
E. Guabá
F. Watershed averages
Suspended solids, in milligrams per liter
Runoff rate, in millimeters per hour
100,000
10,000
1,000
100
10
1
0.1
0.01
25
50
75
90
95
EXPLANATION
Runoff recurrence
LOADEST
Canóvanas
Cayaguás
Guabá
Icacos
Mameyes
Rising stage
Falling stage
Calcite
High chloride
High potassium
Low silica
Canóvanas
Cayaguás
Guabá
Icacos
Mameyes

Figure 12 (facing page). Runoff rate–concentration graphs for suspended sediment. Additional sample characteristics are indicated with black symbols; calcite, samples supersaturated with respect to calcite; high chloride, samples with exceptionally high chloride concentrations collected during huge storms; high potassium, samples with high potassium but not high chloride; low silica, Icacos and Guabá samples with unusually low silica concentrations for the runoff rate. The points separated from the watershed-average curves (F) represent the averages of the classes of sample indicated by the superimposed character.

most abundant bedrock-derived ion, Ca^{2+}. This finding is not consistent with a single common slope for all bedrock-derived constituents. For each river, however, the slopes of the ionic constituents are ranked according to the relative contribution of bedrock and seasalt, from most negative to least negative, Ca^{2+}, Mg^{2+}, Na^{+}, and Cl^{-}. After excluding the high-Cl^{-} storms, chloride has a slope of −0.20 to −0.14. Chloride is atmospherically derived, so this trend must be caused by the mixing of old, evaporated soil waters with younger, typically more dilute rainwater. Focusing on $Si(OH)_4$, Ca^{2+}, and Mg^{2+} to limit seasalt effects, the slopes of the linear relations for granitic rivers are consistently less than for the volcaniclastic rivers, suggesting that the physics of water flow through the different soils is slightly different and grouped by geology. A precise physical explanation is limited by the inability to measure, in the field, the parameters that contribute to C_1 in the permeability-porosity-aperture model.

The strongly bioactive constituents typically demonstrate two types of concentration-runoff relations. Some of the bioactive constituents have nearly constant runoff-rate–to–concentration relations (a chemostat), ordinarily with considerable scatter. For DOC, and for some of the remaining bioactive constituents in some rivers, concentrations increase as runoff increases, until runoff rates reach between 3 and 10 mm h^{-1}. At still higher runoff rates, concentrations decrease. This sequence can be interpreted in terms of a simplified soil-hydrology model. At low discharge, most water is presumably arriving through deeper flow paths with less-available bioactive constituents. With increasing runoff, flow paths are more shallow, more-available constituents are removed, and concentrations rise. At the highest runoff, overland flow and macropore flow become important. These paths have less contact with the soil matrix and do not generate waters high in bioactive constituent concentrations; accordingly, stream concentrations drop. An alternate explanation, solute depletion during storms, should cause recessions to have lower concentrations than rises. None of the bioactive constituents show this behavior.

Acknowledgements

This work was supported through the United States Geological Survey Water, Energy, and Biogeochemical Budgets program (Larsen and others, 1993; Lins, 1994). This chapter benefited from reviews by Brent Aulenbach, Alisa Mast, and Jamie Shanley. Without the initial groundwork by Angel Torres-Sánchez in the field and Ellen Axtmann in the lab this report would not have been possible.

References

Aitkenhead, J.A., and McDowell, W.H., 2000, Soil C : N ratio as a predictor of annual riverine DOC flux at local and global scales: Global Biogeochemical Cycles, v. 14, no. 1, p. 127–138.

Andreae, M.O., and Andreae, T.W., 1988, The cycle of biogenic sulfur-compounds over the Amazon Basin—1. Dry season: Journal of Geophysical Research—Atmospheres, v. 93, p. 1487–1497.

Beven, K.J., and Germann, P., 1982, Macropores and water flows in soils: Water Resources Research, v. 18, p. 1311–1325.

Bevington, P.R., and Robinson, K.D., 2003, Data reduction and error analysis for the physical sciences—2: New York, McGraw Hill, 320 p.

Bhatt, M.P., and McDowell, W.H., 2007, Controls on major solutes within the drainage network of a rapidly weathering tropical watershed: Water Resources Research, v. 43, p. 1–9.

Brantley, S.L., Crane, S.R., Crerar, D.A., Hellmann, R., and Stallard, R.F., 1986, Dissolution at dislocation etch pits in quartz: Geochimica et Cosmochimica Acta, v. 50, p. 2349–2361.

Brown, E.T., Stallard, R.F., Larsen, M.C., Bourlès, D.L., Raisbeck, G.M., and Yiou, F., 1998, Determination of predevelopment denudation rates of an agricultural watershed (Cayaguás River, Puerto Rico) using in-situ-produced ^{10}Be in river-borne quartz: Earth and Planetary Science Letters, v. 160, p. 723–728.

Brown, E.T., Stallard, R.F., Larsen, M.C., Raisbeck, G.M., and Yiou, F., 1995, Denudation rates determined from the accumulation of in situ-produced ^{10}Be in the Luquillo Experimental Forest, Puerto Rico: Earth and Planetary Science Letters, v. 129, p. 193–202.

Burrowes, P.A., Joglar, R.L., and Green, D.E., 2004, Potential causes for amphibian declines in Puerto Rico: Herpetologica, v. 60, no. 2, p. 141–154.

Chappell, N.A., Franks, S.W., and Larenus, J., 1998, Multi-scale permeability estimation for a tropical catchment: Hydrological Processes, v. 12, p. 1507–1523.

Chappell, N.A., and Sherlock, M.D., 2005, Contrasting flow pathways within tropical forest slopes of Ultisol soils: Earth Surface Processes and Landforms, v. 30, p. 735–753.

Chestnut, T.J., and McDowell, W.H., 2000, C and N dynamics in the riparian and hyporheic zones of a tropical stream, Luquillo Mountains, Puerto Rico: Journal of the North American Benthological Society, v. 19, p. 199–214.

Chestnut, T.J., Zarin, D.J., McDowell, W.H., and Keller, M., 1999, A nitrogen budget for late-successional hillslope, Tabonuco Forest, Puerto Rico: Biogeochemistry, v. 46, no. 1–3, p. 85–108.

Clark, J.J., and Wilcock, P.R., 2000, Effects of land-use change on channel morphology in northeastern Puerto Rico: Geological Society of America Bulletin, v. 112, p. 1763–1777.

Derry, L.A., Pett-Ridge, J.C., Kurtz, A.C., and Troester, J.W., 2006, Ge/Si and $^{87}Sr/^{86}Sr$ tracers of weathering reactions and hydrologic pathways in a tropical granitoid system: Journal of Geochemical Exploration, v. 88, p. 271–274.

Devol, A.H., Forsberg, B.R., Richey, J.E., and Pimentel, T.P., 1995, Seasonal-variation in chemical-distributions in the Amazon (Solimões) River—A multiyear time-series: Global Biogeochemical Cycles, v. 9, no. 3, p. 307–328.

Edmond, J.M., Palmer, M.R., Measures, C.I., Brown, E.T., and Huh, Y., 1996, Fluvial geochemistry of the eastern slope of the northeastern Andes and its foredeep in the drainage of the Orinoco in Colombia and Venezuela: Geochimica et Cosmochimica Acta, v. 60, no. 16, p. 2949–2976.

Edmond, J.M., Palmer, M.R., Measures, C.I., Grant, B., and Stallard, R.F., 1995, The fluvial geochemistry and denudation rate of the Guayana shield in Venezuela, Colombia, and Brazil: Geochimica et Cosmochimica Acta, v. 59, no. 16, p. 3301–3325.

Elsenbeer, Helmut, 2001, Hydrologic flowpaths in tropical rainforest soilscapes—A review: Hydrological Processes, v. 15, p. 1751–1759.

Elsenbeer, Helmut, and Cassel, D.K., 1990, Surficial processes in the rainforest of western Amazonia, *in* Ziemer, R.R., and O'Loughlin, C.L.H.L.S., eds., Research needs and applications to reduce erosion and sedimentation in tropical steeplands: International Association of Hydrologic Sciences, p. 289–297.

Elsenbeer, Helmut, and Lack, A., 1996, Hydrometric and hydrochemical evidence for fast flowpaths at La Cuenca, western Amazonia: Journal of Hydrology, v. 180, p. 237–250.

Elsenbeer, Helmut, Lack, A., and Cassel, K., 1996, The stormflow chemistry at La Cuenca, western Amazonia: Interciencia, v. 21, p. 133–138.

Fox, L.E., 1989, A model for inorganic control of phosphate concentrations in river waters: Geochimica et Cosmochimica Acta, v. 53, p. 417–428.

Fox, L.E., 1993, The chemistry of aquatic phosphate—Inorganic processes in rivers: Hydrobiologia, v. 253, p. 1–16.

Gibbs, R.J., 1967, The geochemistry of the Amazon River system—I. The factors that control the salinity and composition and concentration of suspended solids: Geological Society of America Bulletin, v. 78, p. 1203–1232.

Gibbs, R.J., 1972, Water chemistry of the Amazon River: Geochimica et Cosmochimica Acta, v. 36, p. 1061–1066.

Godsey, S.E., Elsenbeer, H., and Stallard R.F., 2004, Overland flow generation in two lithologically distinct rainforest watersheds: Journal of Hydrology, v. 295, p. 276–290.

Godsey, S.E., Kirchner J.W., and Clow, D.W., 2009, Concentration-discharge relationships reflect chemostatic characteristics of US watersheds: Hydrological Processes, v. 23, p. 1844–1864.

Gould, W.A., Martinuzzi, S., and Parés-Ramos, I.K., 2012, Land use, population dynamics, and land-cover change in northeastern Puerto Rico, ch. B *in* Murphy, S.F., and Stallard, R.F., eds., Water quality and landscape processes of four watersheds in eastern Puerto Rico: U.S. Geological Survey Professional Paper 1789, p. 25–42.

Haire, W.J., 1972, Flood of October 5–10, 1970, in Puerto Rico: Commonwealth of Puerto Rico Water-Resources Bulletin 12, 42 pages.

Heartsill-Scalley, Tamara, Scatena, F.N., Estrada, C., McDowell, W.H., and Lugo, A.E., 2007, Disturbance and long-term patterns of rainfall and throughfall nutrient fluxes in a subtropical wet forest in Puerto Rico: Journal of Hydrology, v. 333, p. 472–485.

Herrera, Rafael, Jordan, C., Klinge, H., and Medina, E., 1978a, Amazon ecosystems—Their structure and functioning with particular emphasis on nutrients: Interciencia, v. 3, p. 223–232.

Herrera, Rafael, Merida, T., Stark, N., and Jordan, C., 1978b, Direct phosphorus transfer from leaf litter to roots: Naturwissenschaften, v. 65, p. 208–209.

Herwitz, S.R., Muhs, D.R., Prospero, J.M., Mahan, S., and Vaugn, B., 1996, Origin of Bermuda's clay-rich Quaternary paleosols and their paleoclimatic significance: Journal of Geophysical Research, v. 101, no. D18, p. 23,389–23,400.

Johnson, N.M., Likens, G.E., Bormann, F.H., Fisher, D.W., and Pierce, R.S., 1969, A working model for the variation in stream water chemistry at the Hubbard Brook Experimental Forest, New Hampshire: Water Resources Research, v. 5, p. 1353–1363,

Johnsson, M.J., 1990, Tectonic versus chemical-weathering controls on the composition of fluvial sands in tropical environments: Sedimentology, v. 37, p. 713–726.

Johnsson, M.J., and Stallard, R.F., 1989, Physiographic controls on sediments derived from volcanic and sedimentary terrains on Barro Colorado Island, Panama: Journal of Sedimentary Petrology, v. 59, p. 768–781.

Jolly, W.T., Lidiak, E.G., Dickin, A.P., and Wu, T.-W., 1998, Geochemical diversity of Mesozoic island arc tectonic blocks in eastern Puerto Rico, *in* Lidiak, E.G., and Larue, D.K., eds., Tectonics and geochemistry of the northeastern Caribbean: Geological Society of America Special Paper 322, p. 67–98.

Kinner, D.A., and Stallard, R.F., 2004, Identifying storm flow pathways in a rainforest catchment using hydrological and geochemical modeling: Hydrological Processes, v. 18, no. 15, p. 2851–2876.

Langbein, W.B., and Dawdy, D.R., 1964, Occurrence of dissolved solids in surface waters in the United States: U.S. Geological Survey Professional Paper 501–D, p. D115–D117.

Larsen, M.C., 1997, Tropical geomorphology and geomorphic work—A study of geomorphic processes and sediment and water budgets in montane humid-tropical forested and developed watersheds, Puerto Rico: Boulder, University of Colorado Geography Department, Ph.D. dissertation, 341 p.

Larsen, M.C., 2012, Landslides and sediment budgets in four watersheds in eastern Puerto Rico, ch. F *in* Murphy, S.F., and Stallard, R.F., eds., Water quality and landscape processes of four watersheds in eastern Puerto Rico: U.S. Geological Survey Professional Paper 1789, p. 153–178.

Larsen, M.C., Collar, P.D., and Stallard, R.F., 1993, Research plan for the investigation of water, energy, and biogeochemical budgets in the Luquillo Mountains, Puerto Rico: U.S. Geological Survey Open-File Report 92–150, 19 p.

Larsen, M.C., Liu, Z., and Zou, X., 2012, Effects of earthworms on slopewash, surface runoff, and fine-litter transport on a humid tropical forested hillslope, Luquillo Experimental Forest, Puerto Rico, ch. G *in* Murphy, S.F., and Stallard, R.F., eds., Water quality and landscape processes of four watersheds in eastern Puerto Rico: U.S. Geological Survey Professional Paper 1789, p. 179–198.

Larsen, M.C., and Parks, J.E., 1997, How wide is a road? The association of roads and mass-wasting disturbance in a forested montane environment: Earth Surface Processes and Landforms, v. 22, p. 835–848.

Larsen, M.C., and Santiago-Román, A., 2001, Mass wasting and sediment storage in a small montane watershed—An extreme case of anthropogenic disturbance in the humid tropics, *in* Dorava, J.M., Palcsak, B.B., Fitzpatrick, F., and Montgomery, D., eds., Geomorphic processes and riverine habitat: American Geophysical Union Water Science and Application Series, v. 4, p. 119–138.

Larsen, M.C., and Stallard, R.F., 2000, Water, energy, and biogeochemical budgets, Luquillo Mountains, Puerto Rico: U.S. Geological Survey Fact Sheet 163–99, 4 p.

Lewis, W.M., Jr., Hamilton, S.K., Jones, S.L., and Runnells, D.D., 1987, Major element chemistry, weathering, and element yields for the Caura River drainage, Venezuela: Biogeochemistry, v. 4, p. 159–181.

Lewis, W.M., Jr., and Saunders, J.F., III, 1989, Concentration and transport of dissolved and suspended substances in the Orinoco River: Biogeochemistry, v. 7, p. 203–240.

Lewis, W.M., Jr., and Saunders, J.F., III, 1990, Chemistry and element transport by the Orinoco main stem and lower tributaries, *in* Weibezahn, F.H., Alvarez, H., and Lewis, W.M., Jr., eds., El Río Orinoco como ecosistema / The Orinoco River as an ecosystem: Caracas, Venezuela, Impresos Rubel, p. 211–239, 430 p.

Lins, H.F., 1994, Recent directions taken in water, energy, and biogeochemical budget research: Eos, Transactions, American Geophysical Union, v. 75, no. 38, p. 433, 438–439.

Lodge, D.J., McDowell, W.H., and McSwiney, C.P., 1994, The importance of nutrient pulses in tropical forests: Trends in Ecology & Evolution, v. 9, p. 384–387.

Lugo, A.E., and Frangi, J.L., 2003, Changes in necromass and nutrients on the forest floor of a palm floodplain forest in the Luquillo Mountains of Puerto Rico: Caribbean Journal of Science, v. 39, no. 3, p. 265–272.

McDowell, W.H., 1991, Nutrient and major element chemistry of Caribbean rain forests streams: Internationale Vereinigung für theoretische und angewandte Limnologie, v. 24, p. 1720–1723.

McDowell, W.H., 1998, Internal nutrient fluxes in a Puerto Rican rain forest: Journal of Tropical Ecology, v. 14, p. 521–536.

McDowell, W.H., 2001, Hurricanes, people and riparian zones—Controls on nutrient losses from forested Caribbean watersheds: Forest Ecology and Management, v. 154, p. 443–451

McDowell, W.H., and Asbury, C.E., 1994, Export of carbon, nitrogen, and major ions from three tropical montane watersheds: Limnology and Oceanography, v. 39, p. 111–125.

McDowell, W.H., Gines-Sanchez, C., Asbury, C.E., and Ramos Perez, C.R., 1990, Influence of sea-salt aerosols and long-range transport on precipitation chemistry at El Verde, Puerto Rico: Atmospheric Environment, v. 24A, p. 2813–2821.

McDowell, W.H., McSwiney, C.P., and Bowden, W.B., 1996, Effects of hurricane disturbance on groundwater chemistry and riparian function in a tropical rain forest: Biotropica, v. 28, p. 577–584.

Murphy, S.F., and Stallard, R.F., 2012, Hydrology and climate of four watersheds in eastern Puerto Rico, ch. C *in* Murphy, S.F., and Stallard, R.F., eds., Water quality and landscape processes of four watersheds in eastern Puerto Rico: U.S. Geological Survey Professional Paper 1789, p. 43–84.

Murphy, S.F., Stallard, R.F., Larsen, M.C., and Gould, W.A., 2012, Physiography, geology, and land cover of four watersheds in eastern Puerto Rico, ch. A *in* Murphy, S.F., and Stallard, R.F., eds., Water quality and landscape processes of four watersheds in eastern Puerto Rico: U.S. Geological Survey Professional Paper 1789, p. 1–24.

Ostertag, Rebecca, Scatena, F.N., and Silver, W.L., 2003, Forest floor decomposition following hurricane litter inputs in several Puerto Rican forests: Ecosystems, v. 6, p. 261–273.

Peters, N.E., Shanley, J.B., Aulenbach, B.T., Webb, R.M., Campbell, D.H., Hunt, R., Larsen, M.C., Stallard, R.F., Troester, J., Walker, J.F., 2006, Water and solute mass balance of five small, relatively undisturbed watersheds in the U.S.: Science of the Total Environment, v. 358, p. 221–242.

Pett-Ridge, J.C., 2009, Contributions of dust to phosphorus cycling in tropical forests of the Luquillo Mountains, Puerto Rico: Biogeochemistry, v. 96, no. 1, p. 63–80.

Pett-Ridge, J.C., Derry, L.A., and Barrows, J.K., 2009a, Ca/Sr and $^{87}Sr/^{86}Sr$ ratios as tracers of Ca and Sr cycling in the Río Icacos watershed, Luquillo Mountains, Puerto Rico: Chemical Geology, v. 94, no. 1, p. 64–80.

Pett-Ridge, J.C., Derry, L.A., and Kurtz, A.C., 2009b, Sr isotopes as a tracer of weathering processes and dust inputs in a tropical granitoid watershed, Luquillo Mountains, Puerto Rico: Geochimica et Cosmochimica Acta, v. 73, p. 25–43.

Reid, E.A., Reid, J.S., Meier, M.M., Dunlap, M.R., Cliff, S.S., Broumas, A., Perry, K., and Maring, H., 2003, Characterization of African dust transported to Puerto Rico by individual particle and size segregated bulk analysis: Journal of Geophysical Research, v. 108, no. D19, 8591, p. 1–22.

Runkel, R.L., Crawford, C.G., and Cohn, T.A., 2004, Load Estimator (LOADEST)—A FORTRAN program for estimating constituent loads in streams and rivers: U.S. Geological Survey Techniques and Methods Book 4, ch. A5, 69 p., program, test files.

Saunders, J.F., III, and Lewis, W.M., Jr., 1988, Transport of phosphorus, nitrogen, and carbon by the Apure River, Venezuela: Biogeochemistry, v. 5, p. 323–342.

Saunders, J.F., III, and Lewis, W.M., Jr., 1989, Transport of major solutes and the relationship between solute concentrations and discharge in the Apure River, Venezuela: Biogeochemistry, v. 8, p. 101–113.

Schaefer, D.A., McDowell, W.H., Scatena, F.N., and Asbury, C.E., 2000, Effects of hurricane disturbance on stream water concentrations and fluxes in eight tropical forest watersheds of the Luquillo Experimental Forest, Puerto Rico: Journal of Tropical Ecology, v. 16, p. 189–207.

Schulz, M.S., and White, A.F., 1999, Chemical weathering in a tropical watershed, Luquillo Mountains, Puerto Rico. III. Quartz dissolution rates: Geochimica et Cosmochimica Acta, v. 63, no. 3–4, p. 337–350.

Shanley, J.B., McDowell, W.H., and Stallard, R.F., 2011, Long-term patterns and short-term dynamics of stream solutes and suspended sediment in a rapidly weathering tropical watershed: Water Resources Research, v. 47, no. W07515, p. 1–11.

Simon, Andrew, Larsen, M.C., and Hupp, C.R., 1990, The role of soil processes in determining mechanisms of slope failure and hillslope development in a humid-tropical forest, eastern Puerto Rico, *in* Kneuper, P.L.K., and McFadden, L.D., eds., Soils and landscape evolution. Geomorphology, v. 3, p. 263–286.

Smith, A.L., Shellekens, J.H., and Diaz, A.-L.M., 1998, Batholiths as markers of tectonic change in the northeastern Caribbean, *in* Lidiak, E.G., and Larue, D.K., eds., Tectonics and geochemistry of the northeastern Caribbean: Geological Society of America Special Paper 322, p. 99–122.

Soil Survey Staff, 1995, Order 1 soil survey of the Luquillo Long-Term Ecological Research Grid, Puerto Rico: Lincoln, Nebraska, U.S. Department of Agriculture Natural Resources Conservation Service, 93 p.

Stallard, R.F., 1985, River chemistry, geology, geomorphology, and soils in the Amazon and Orinoco basins, *in* Drever, J.I., ed., The chemistry of weathering: Dordrecht, Holland, D. Reidel Publishing Company, NATO ASI Series C—Mathematical and Physical Sciences, v. 149, p. 293–316.

Stallard, R.F., 1988, Weathering and erosion in the humid tropics, *in* Lerman, Abraham, and Meybeck, M., eds., Physical and chemical weathering in geochemical cycles: Dordrecht, Holland, Kluwer Academic Publishers, NATO ASI Series C—Mathematical and physical sciences 251, p. 225–246.

Stallard, R.F., 1995a, Relating chemical and physical erosion, *in* White, A.F., and Brantley, S.L. eds., Chemical weathering rates of silicate minerals: Reviews in Mineralogy, v. 31, p. 543–564.

Stallard, R.F., 1995b, Tectonic, environmental, and human aspects of weathering and erosion—A global review using a steady-state perspective: Annual Review of Earth and Planetary Sciences, v. 12, p. 11–39.

Stallard, R.F., 2001, Possible environmental factors underlying amphibian decline in eastern Puerto Rico—Analysis of U.S. government data archives: Conservation Biology, v. 15, p. 943–953.

Stallard, R.F., 2012a, Atmospheric inputs to watersheds in the Luquillo Mountains of eastern Puerto Rico, ch. D *in* Murphy, S.F., and Stallard, R.F., eds., Water quality and landscape processes of four watersheds in eastern Puerto Rico: U.S. Geological Survey Professional Paper 1789, p. 85–112.

Stallard, R.F., 2012b, Weathering, landscape equilibrium, and carbon in four watersheds in eastern Puerto Rico, ch. H *in* Murphy, S.F., and Stallard, R.F., eds., Water quality and landscape processes of four watersheds in eastern Puerto Rico: U.S. Geological Survey Professional Paper 1789, p. 199–248.

Stallard, R.F., and Edmond, J.M., 1981, Geochemistry of the Amazon—1. Precipitation chemistry and the marine contribution to the dissolved load at the time of peak discharge: Journal of Geophysical Research—Oceans and Atmospheres, v. 86, no. NC10, p. 9844–9858.

Stallard, R.F., and Edmond, J.M., 1983, Geochemistry of the Amazon—2. The influence of the geology and weathering environment on the dissolved load: Journal of Geophysical Research—Oceans and Atmospheres, v. 88, no. NC14, p. 9671–9688, microfiche supplement.

Stallard, R.F., and Edmond, J.M., 1987, Geochemistry of the Amazon—3. Weathering chemistry and limits to dissolved inputs: Journal of Geophysical Research—Oceans, v. 92, no. C8, p. 8293–8302.

Stallard, R.F., Koehnken, L., and Johnsson, M.J., 1991, Weathering processes and the composition of inorganic material transported through the Orinoco River system, Venezuela and Colombia: Geoderma, v. 51, no. 1–4, p. 133–165.

Stark, Nellie, and Jordan, C.F., 1978, Nutrient retention by the root mat of an Amazonian rain forest: Ecology, v. 59, p. 434–437.

Stumm, Werner, and Morgan, J.J., 1981, Aquatic chemistry: New York, John Wiley, 780 p.

Tardy, Yves, Bustillo, V., Roquin, C., Mortatti, J., and Victoria, R., 2005, The Amazon—Bio-geochemistry applied to river basin management—1. Hydro-climatology, hydrograph separation, mass transfer balances, stable isotopes, and modelling: Applied Geochemistry, v. 20, p. 1746–1829.

Tardy, Yves, Roquin, C., Bustillo, V., Moreira, M., Martinelli, L.A., and Victoria, R., 2009, Carbon and water cycles—Amazon River basin applied biogeochemistry: Biarritz, France, Atlantica Seguier, 480 p.

Webb, R.M.T., and Soler-López, L.R., 1997, Sedimentation history of Lago Loíza, Puerto Rico, 1953–94: U.S. Geological Survey Water-Resources Investigations Report 97–4108, 18 p.

Wolman, M.G., and Miller, J.P., 1960, Magnitude and frequency of forces in geomorphic processes: Journal of Geology, v. 68, p. 54–74.

Ziegler, Karen, Chadwick, O.A., White, A.F., and Brzezinski, M.A., 2005, δ^{30}Si systematics in a granitic saprolite, Puerto Rico: Geology, v. 33, no. 10, p. 817–820.